Supplement of Atmos. Chem. Phys., 19, 379–405, 2019
https://doi.org/10.5194/acp-19-379-2019-supplement

Atmospheric Chemistry and Physics
Open Access
EGU

Supplement of

An evaluation of European nitrogen and sulfur wet deposition and their trends estimated by six chemistry transport models for the period 1990–2010

Mark R. Theobald et al.

Correspondence to: Mark R. Theobald (mark.theobald@ciemat.es)

S1 Analysis of the errors in wet deposition due to errors in the primary particulate matter emissions

Errors were found in the emissions of primary particulate matter for Russia and North African countries and shipping for the period 1991-1999. Unfortunately it was not possible to re-run the simulations since these errors were not detected until late in the data analysis. In order to estimate the impact on the wet deposition estimates, the CHIMERE model was used to simulate wet deposition using the incorrect and corrected emissions for 1998, the year for which the emission error is the largest. Figure S1 shows the relative errors in the model estimates of WNOx, WNHx and WSOx as a result of the errors in emissions. Errors in WNOx and WSOx were less than 0.5% in most of the domain with maximum errors of 0.95% and 1.5%, respectively. Errors in WNHx were also mostly below 0.5% but larger errors were estimated for about a quarter of the domain (mostly in the northeast), with a maximum error of 2.4%. These errors are small compared with the overall uncertainty of the model estimates and the uncertainty of the observations. Errors in the trends calculated from the simulations with erroneous emissions are expected to be smaller than the errors in annual deposition rates. From this analysis we conclude that the error in emissions is unlikely to affect the results and conclusions of the study significantly.

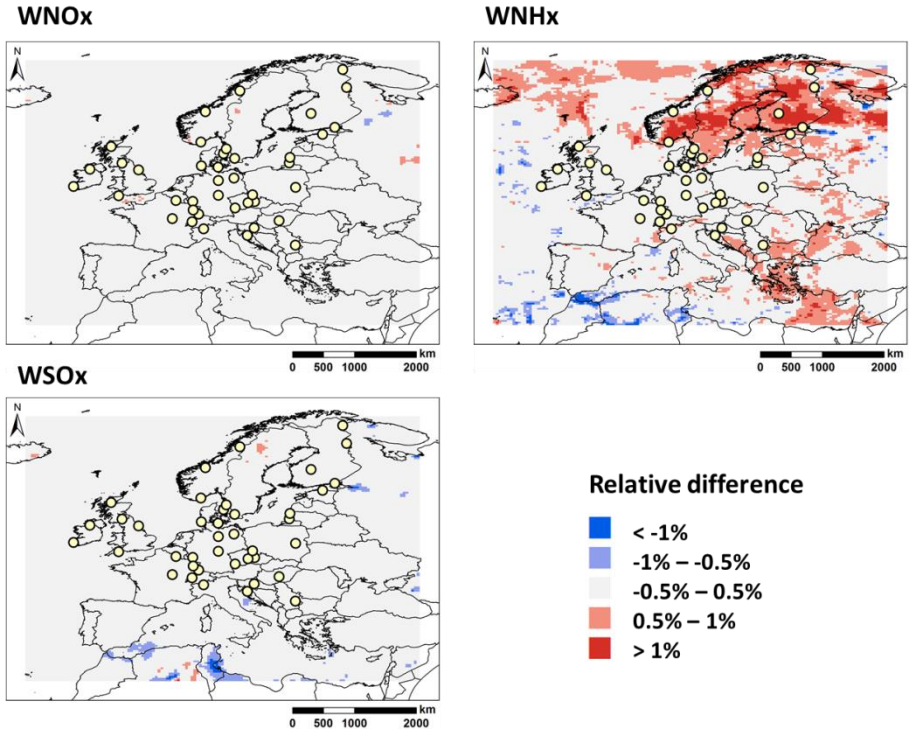

Figure S1: Maps of relative difference between the model estimates of WNOx, WNHx and WSOx for the simulations using the original (incorrect) emissions and those using the corrected emissions of primary PM in Russia, North Africa and maritime areas for 1998. Circles show the locations of the sites used to evaluate modelled deposition. Note: Positive values indicate that the emission error resulted in larger values of wet deposition and vice versa.

S2 Table and Figures cited in the article

Table S1: Main features of the chemistry-transport models involved in the EURODELTA-Trends deposition modelling exercise (Adapted from Colette et al., 2017a).

Model	**CHIMERE (CHIM)**	**CMAQ**	**EMEP MSC-W (EMEP)**	**LOTOS-EUROS (LOTO)**	**MATCH**	**MINNI**
Version / Date	Modified CHIMERE2013	V5.0.2	rv4.7 spring 2015	v1.10.005	VSOA April 2016	V4.7
Operator	INERIS	BSC	MET Norway	TNO	SMHI	ENEA/Arianet S.r.l.
Name and resolution of the meteorological driver	WRF with nudging (common driver) 0.44°	WRF (no nudging) 25 km	WRF with nudging (common driver) 0.44°	RACMO2 0.22°	HIRLAM EURO4M reanalysis Approx. 22 km	WRF with nudging (common driver) 0.44°
Vertical layers of CTM	9 sigma	15 sigma	20 sigma	5 (4 dynamic layers and a surface layer)	39 hybrid levels of the meteorological model layers	16 fixed terrain-following layers
Vertical extent of CTM	500 hPa	50 hPa	100 hPa	5000 m	ca. 5000 m (4700–6000 m)	10 000m
Surface concentration height	10 m (midpoint of first model layer)	20 m (midpoint of first model layer)	Downscaled to 3 m	Downscaled to 3 m	Downscaled to 3 m	20 m (midpoint of first model layer)
Land-use database	GLOBCOVER (24 classes)	Corine Land Cover 2006 (44 classes)	CCE/SEI for Europe, elsewhere GLC2000	Corine Land Cover 2000 (13 classes)	CCE/SEI for Europe	Corine Land Cover 2006 (22 classes)

Model	CHIMERE (CHIM)	CMAQ	EMEP MSC-W (EMEP)	LOTOS-EUROS (LOTO)	MATCH	MINNI
Dry deposition	Resistance model (Emberson et al., 2000a, b)	Multiple resistance analogy for gases (Pleim and Xiu, 1995) and electrical analogy for aerosol (Venkatram and Pleim, 1999)	Resistance model for gases (Venkatram and Pleim, 1999); for aerosols: Simpson et al. (2012)	Resistance model, DEPAC3.11 for gases, Van Zanten et al. (2010) and Zhang et al. (2001) for aerosols	Resistance model depending on aerodynamic resistance and land use (vegetation). Similar to Andersson et al. (2007)	Resistance model based on Wesely (1989)
Ammonia compensation points	None	Bidirectional NH_3 model (Pleim et al., 2013) – not used in this study	None, but zero NH_3 deposition over growing crops	Only for stomatal, external leaf surface and soil (=0))	None	None
Stomatal resistance	Emberson et al. (2000a, b)	Pleim-Xiu Land Surface Model (Pleim and Xiu, 2003)	DO3SEEMEP: Emberson et al. (2000a, b), Tuovinen et al. (2004), Simpson et al. (2012)	Emberson et al. (2000a, b)	Simple, seasonally varying, diurnal variation of surface resistance for gases with stomatal resistance (similar to Andersson et al., 2007)	Wesely (1989)
Wet deposition - gases	In-cloud and sub-cloud scavenging coefficients	Simple first-order process (Chang et al., 1987)	In-cloud and sub-cloud scavenging coefficients (implicit dependence on solubility and particle size)	Sub-cloud scavenging coefficient (no in-cloud scavenging)	In-cloud scavenging of some species based on Henry's law constants. Simple in-cloud and sub-cloud scavenging coefficients for other gases.	In-cloud and sub-cloud scavenging coefficients (Simpson et al., 2003)

Model	CHIMERE (CHIM)	CMAQ	EMEP MSC-W (EMEP)	LOTOS-EUROS (LOTO)	MATCH	MINNI
Wet deposition – scavenging of gases	In-cloud: Scavenging for O_3, NO, NO_2, NO_3, HNO_3, HCl, NH_3, SO_2, H_2O_2 and several VOCs (according to their Henry's law constant) Sub-cloud: Scavenging of NH_3, HNO_3 and HCl by falling drops Menut et al. (2013); Couvidat et al. (2018)	If the gas participates in cloud chemistry: Scavenging depends on Henry's law constants, dissociation constants, and cloud water pH. If not, the model uses the effective Henry's law equilibrium equation to calculate ending concentrations and deposition amounts Byun and Schere (2006)	Scavenging calculated from the gas mixing ratio, precipitation rate and species-specific scavenging ratios. Different scavenging ratios are used for in-cloud and sub-cloud processes Simpson et al. (2012)	Sub-cloud: Scavenging calculated from the gas mixing ratio, precipitation rate and species-specific scavenging ratios. Simpson et al. (2003) and Scott (1978)	Wet scavenging is assumed to be proportional to the precipitation intensity for most gaseous components. For O3, hydrogen peroxide (H_2O_2) and SO_2, in-cloud scavenging is calculated by assuming Henry's law equilibrium. Sub-cloud scavenging is neglected for these species. The wet scavenging coefficients for SO_2, O_3 and H_2O_2 depend on meteorology. For other species, fixed species-specific coefficients are used. Andersson et al. (2007)	Scavenging calculated from the gas mixing ratio, precipitation rate and species-specific scavenging ratios. Different scavenging ratios are used for in-cloud and sub-cloud processes. Simpson et al. (2003)
Wet deposition - particles	In-cloud and sub-cloud scavenging coefficients	Simple first-order process (Chang et al., 1987)	In-cloud and sub-cloud scavenging coefficients (implicit dependence on solubility and particle size)	Sub-cloud scavenging coefficient (no in-cloud scavenging)	In-cloud and sub-cloud scavenging. Similar to Simpson et al. (2012)	In-cloud and sub-cloud scavenging coefficients (Simpson et al., 2003)

Model	CHIMERE (CHIM)	CMAQ	EMEP MSC-W (EMEP)	LOTOS-EUROS (LOTO)	MATCH	MINNI
Wet deposition – scavenging of particles	In-cloud: particles can be scavenged either by coagulation with cloud droplets or by precipitating drops. Particles also act as cloud condensation nuclei to form new droplets. This latter process of nucleation is the most efficient one in clouds. Sub-cloud: particles are scavenged by raining drops with the deposition flux depending on empirical scavenging coefficients Menut et al. (2013)	The accumulation mode and coarse mode aerosols are assumed to be completely absorbed by the cloud and rain water. The Aitken mode aerosols are treated as interstitial aerosol and are slowly absorbed into the cloud/rain water. Only the equilibrium of the sulphate, nitrate, ammonium, and water system is considered. Byun and Schere (2006)	In-cloud: As gas scavenging above Sub-cloud: Scavenging calculated from the particle mixing ratio, precipitation rate, raindrop fall speed and a size-dependent collection efficiency. Simpson et al. (2012)	Sub-cloud: Scavenging calculated from the particle mixing ratio, precipitation rate, raindrop fall speed and a size-dependent collection efficiency. Simpson et al. (2003) and Scott (1978)	In-cloud scavenging is proportional to the fraction of the cloud water that hits the ground as precipitation. All particulate sulphate inside clouds is assumed to be dissolved to cloud droplets. The wet scavenging coefficients for ammonium sulphate and SO_4^{2-} depend on meteorology. Sub-cloud scavenging for sulphate is calculated as in Berge (1993).	In-cloud: As gas scavenging above Sub-cloud: Scavenging calculated from the particle mixing ratio, precipitation rate, raindrop fall speed and a size-dependent collection efficiency. Simpson et al. (2003)
Gas-phase chemistry	MELCHIOR2	CB-05 with chlorine chemistry extensions (Yarwood et al., 2005)	EmChem09 (Simpson et al., 2012)	TNO-CBM-IV	Based on EMEP (Simpson et al., 2012), with modified isoprene chemistry (Carter, 1996; Langner et al., 1998)	SAPRC99 (Carter, 2000)

Model	CHIMERE (CHIM)	CMAQ	EMEP MSC-W (EMEP)	LOTOS-EUROS (LOTO)	MATCH	MINNI
Cloud chemistry	Aqueous SO_2 chemistry and pH-dependent SO_2 chemistry	Aqueous SO_2 chemistry (Walcek and Taylor, 1986)	Aqueous SO_2 chemistry, pH-dependent	Aqueous SO_2 chemistry, pH-dependent (Banzhaf et al., 2012)	Aqueous SO_2 chemistry	Aqueous SO_2 chemistry (Seinfeld and Pandis, 1998)
Coarse nitrate	No reaction with Ca even if reaction with Na is taken into account. Coarse nitrate might exist with transfer from smaller particles	None	Two formation rates of coarse NO_3 from HNO_3 for relative humidity below/above 90%	Heterogeneous reaction of HNO_3 with coarse sea salt aerosols to obtain $NaNO_3$ Wichink Kruit et al. (2012)	Transfer of HNO_3(g) to aerosol nitrate using rate from Strand and Hov (1994)	None
Ammonium nitrate equilibrium	ISORROPIA v2.1 (Nenes et al., 1999)	ISORROPIA v2.1 (Nenes et al., 1999)	MARS (Binkowski and Shankar, 1995)	ISORROPIA v2 (Nenes et al., 1999)	RH- & T-dependent equilibrium constant (Mozurkewich, 1993)	ISORROPIA v1.7 (Nenes et al., 1999)
Aerosol physics	Coagulation/ condensation/ nucleation Computation of the wet diameter for each size bin as a function of humidity (used for coagulation, condensation, deposition)	Coagulation/ condensation/ nucleation	Not used here	Not used here	Not used here	Coagulation/ condensation/ nucleation

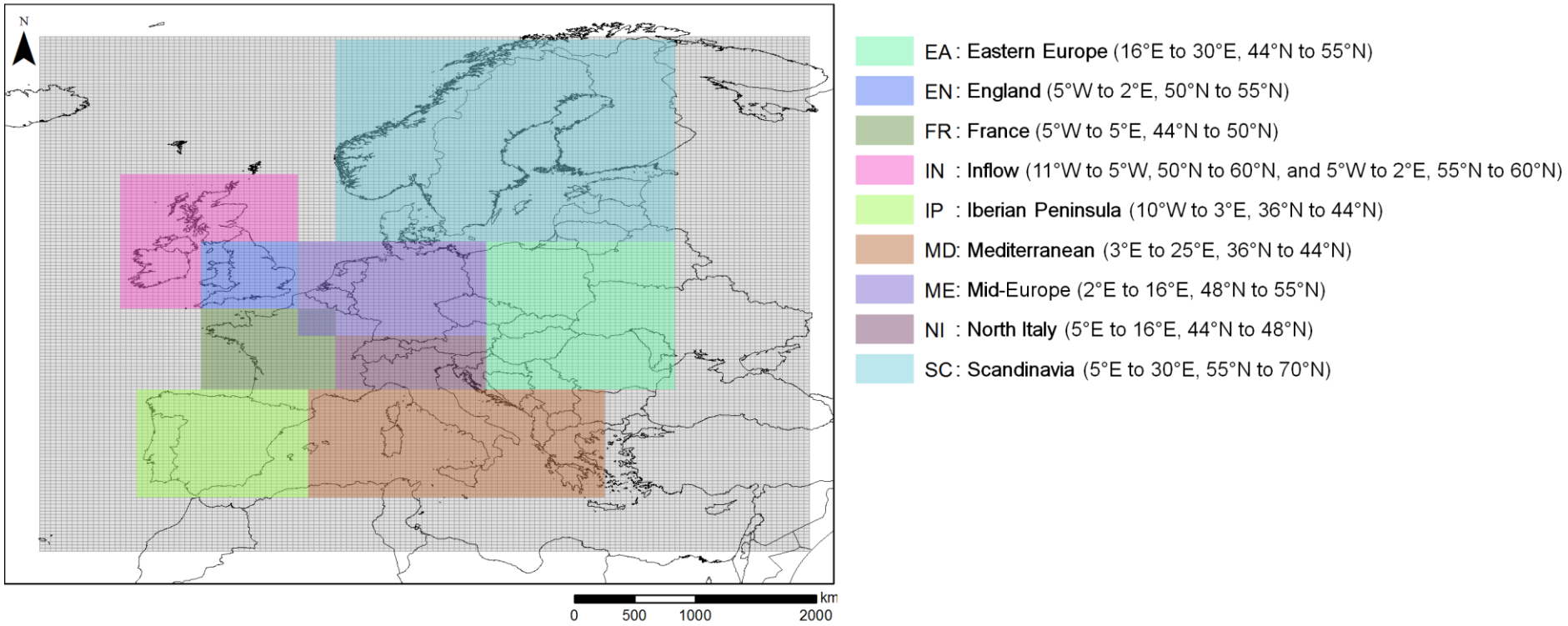

Figure S2: Map showing the grid cells of the modelling domain and the nine sub-regions used in the trend attribution analyses.

Table S2: EMEP stations used for the observations of the various wet deposition and concentration components

Station	Latitude	Longitude	WNOx	WNHx	WSOx	TNO3	TNH4	TSO4	Extra site (2000-2010)
BE0014R	51.12	2.66	•	•					•
CH0002R	46.81	6.94	•	•	•			•	
CH0004R	47.05	6.98	•	•	•				•
CH0005R	47.07	8.46	•	•	•				•
CZ0001R	49.73	16.05	•	•	•			•	
CZ0003R	49.58	15.08	•	•	•		•	•	
DE0001R	54.93	8.31	•	•	•			•	
DE0002R	52.80	10.76	•	•	•			•	
DE0003R	47.91	7.91	•	•	•				
DE0004R	49.76	7.05	•	•	•				
DE0005R	48.82	13.22	•	•	•				
DE0007R	53.17	13.03	•	•	•			•	
DE0008R	50.65	10.77		•					
DE0009R	54.43	12.73	•	•	•				•
DE0044R	51.53	12.93	•	•	•				•
DK0003R	56.35	9.60				•	•		
DK0005R	54.73	10.73	•		•				
DK0008R	56.72	11.52	•	•		•	•		
DK0022R	56.08	9.42		•	•				•
EE0009R	59.50	25.90	•	•					
EE0011R	58.38	21.82	•	•	•				•
ES0007R	37.23	-3.53	•	•	•				•
ES0008R	43.44	-4.85	•	•	•				•
ES0009R	41.28	-3.14	•	•	•				•
ES0011R	38.48	-6.92	•	•	•				•
ES0012R	39.09	-1.10	•	•	•				•
ES0013R	41.28	-5.87	•	•	•				•
ES0016R	43.23	-7.70	•	•	•				•
FI0004R	62.53	24.22	•	•	•	•		•	
FI0009R	59.78	21.38				•	•		
FI0017R	60.53	27.69	•	•	•	•	•	•	
FI0022R	66.32	29.40	•	•	•	•	•	•	
FI0037R	62.58	24.18					•		
FI0053R	65.00	24.69	•	•					•
FR0008R	48.50	7.13	•	•	•				
FR0009R	49.90	4.63	•	•	•				
FR0010R	47.27	4.08	•	•	•				
FR0013R	43.62	0.18	•	•	•				•
FR0014R	47.30	6.83	•	•	•				•
FR0090R	48.52	-4.75	•	•					•
GB0002R	55.31	-3.20	•	•	•				
GB0006R	54.44	-7.87	•	•	•				
GB0013R	50.60	-3.71	•	•	•				

Station	Latitude	Longitude	WNOx	WNHx	WSOx	TNO3	TNH4	TSO4	Extra site (2000-2010)
GB0014R	54.33	-0.81	•	•	•	•	•		
GB0015R	57.73	-4.77	•	•	•				
HR0002R	45.90	15.97	•	•	•				
HR0004R	44.82	14.98	•	•	•				
HU0002R	46.97	19.58	•	•		•	•		
IE0001R	51.94	-10.24	•	•	•			•	
IT0001R	42.10	12.63	•	•	•				•
IT0004R	45.80	8.63	•	•	•			•	
LT0015R	55.35	21.07	•	•	•		•	•	
LV0010R	56.16	21.17	•	•	•			•	
NL0009R	53.33	6.28	•	•	•				•
NL0091R	52.30	4.50	•	•					•
NO0001R	58.38	8.25	•	•	•		•	•	
NO0002R	58.39	8.25				•			
NO0015R	65.83	13.92	•		•			•	
NO0039R	62.78	8.88	•	•	•	•	•	•	
PL0002R	51.82	21.98	•	•	•	•		•	
PL0003R	50.74	15.74	•	•	•		•	•	
PL0004R	54.75	17.53	•	•	•				•
PL0005R	54.15	22.07	•	•	•				•
RS0005R	43.40	21.95	•	•	•				
RU0001R	68.93	28.85	•	•	•				
RU0018R	54.90	37.80	•	•					•
SE0002R	57.42	11.93		•	•			•	
SE0005R	63.85	15.33					•		
SE0011R	56.02	13.15	•	•	•	•	•	•	
SE0014R	57.39	11.91	•			•	•		
SK0004R	49.15	20.28	•	•	•				•
SK0006R	49.05	22.27	•	•	•				•
SK0007R	47.96	17.86	•	•	•				•

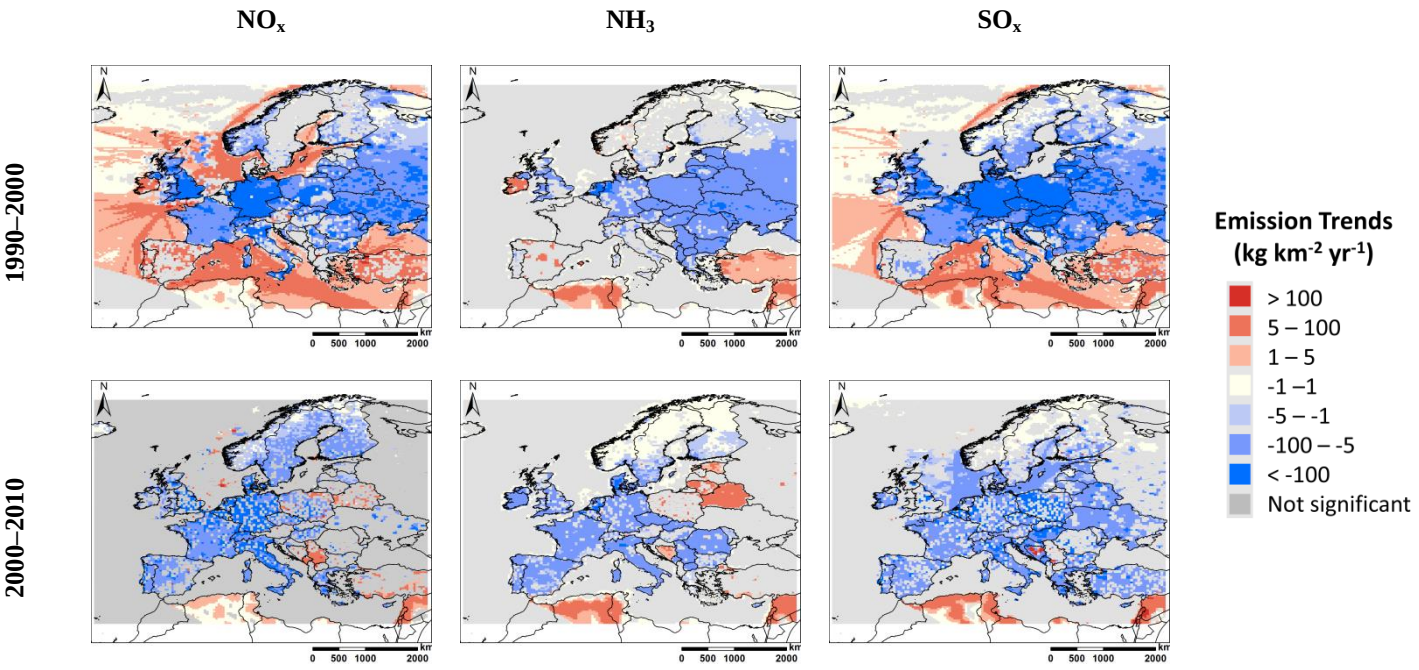

Figure S3: Maps of the trends (Sen's slopes) in the gridded NO_x, NH_3 and SO_x emissions used in the model simulations for the two ten year periods.

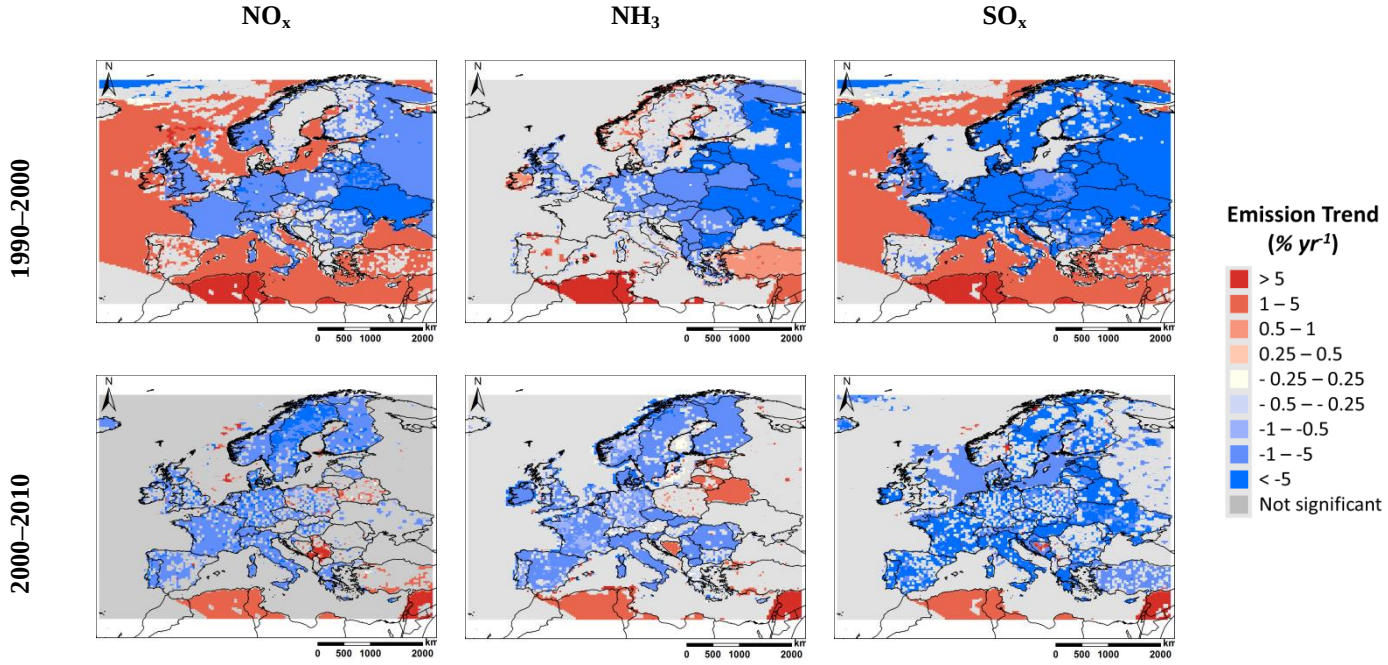

Figure S4: Maps of the relative trends (trend divided by the estimated emission at the beginning of the period) in the gridded NO_x, NH_3 and SO_x emissions used in the model simulations for the two ten year periods.

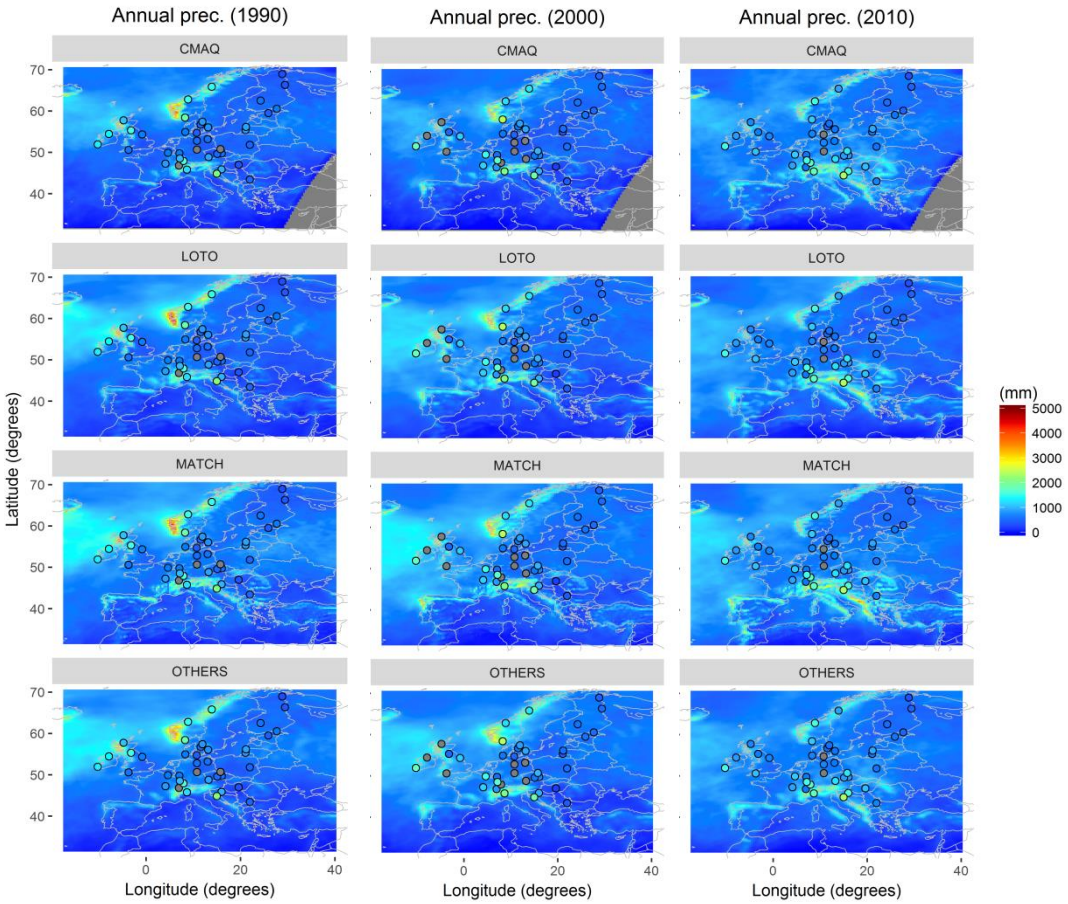

Figure S5: Accumulated annual precipitation estimated by the four meteorological models used in the simulations by CMAQ, LOTO, MATCH and the rest of the models (OTHERS) for the years 1990 (left), 2000 (centre) and 2010 (right). The observed precipitation is shown by the coloured circles (grey indicates no data).

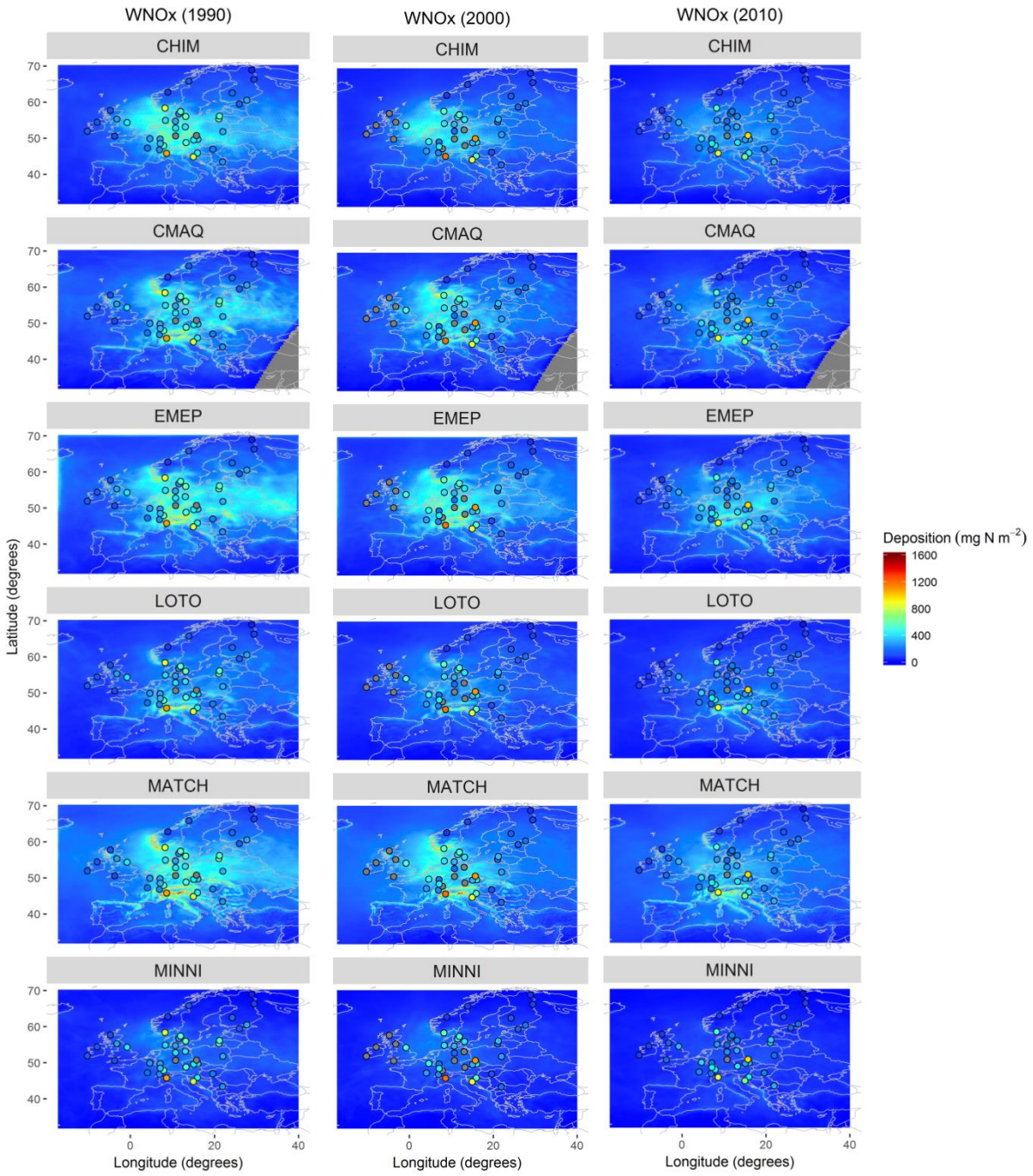

Figure S6: Accumulated annual WNOx deposition estimated by the six models for the years 1990 (left), 2000 (centre) and 2010 (right). The observed deposition is shown by the coloured circles (grey indicates no data).

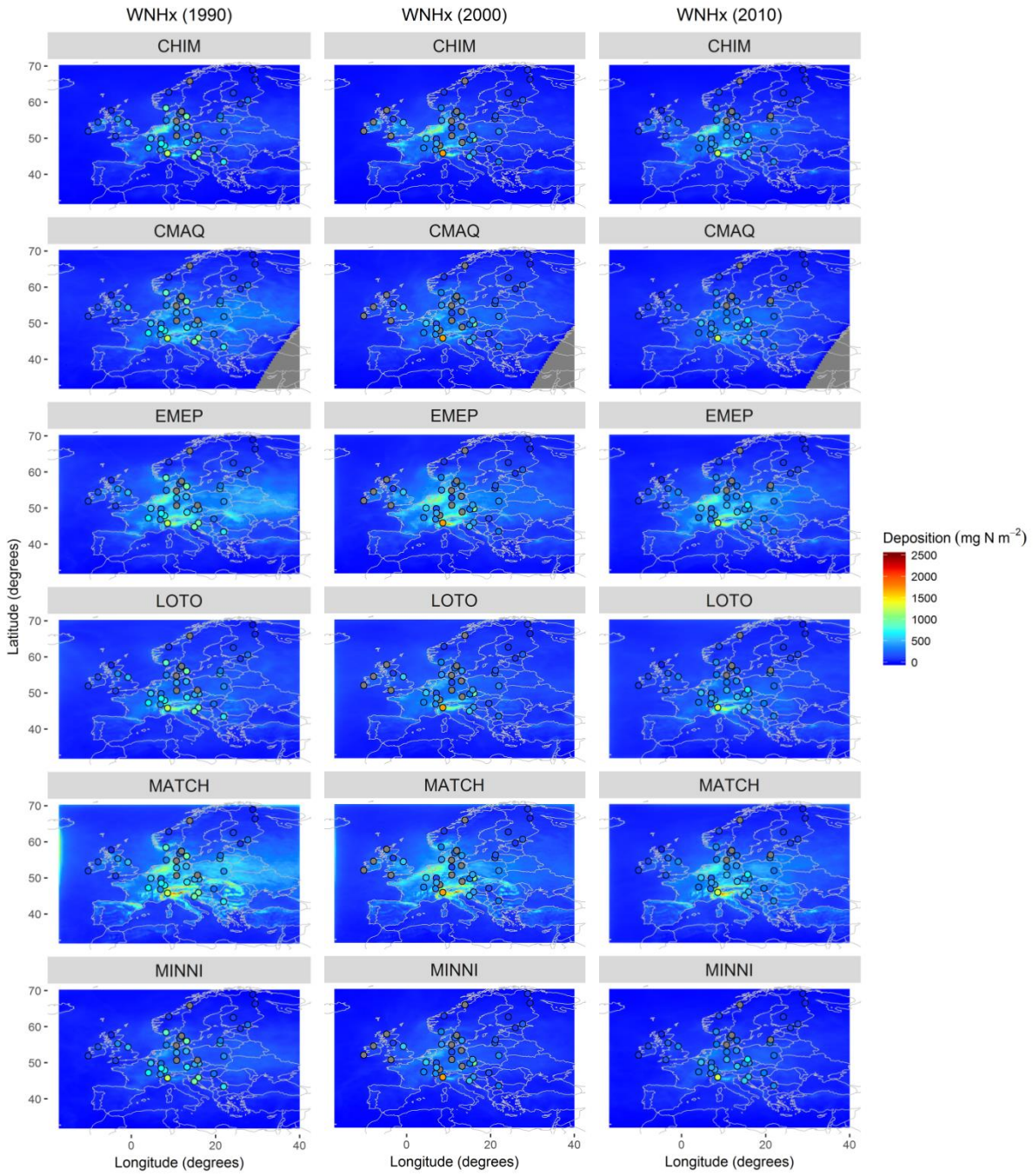

Figure S7: Accumulated annual WNHx deposition estimated by the six models for the years 1990 (left), 2000 (centre) and 2010 (right). The observed deposition is shown by the coloured circles (grey indicates no data).

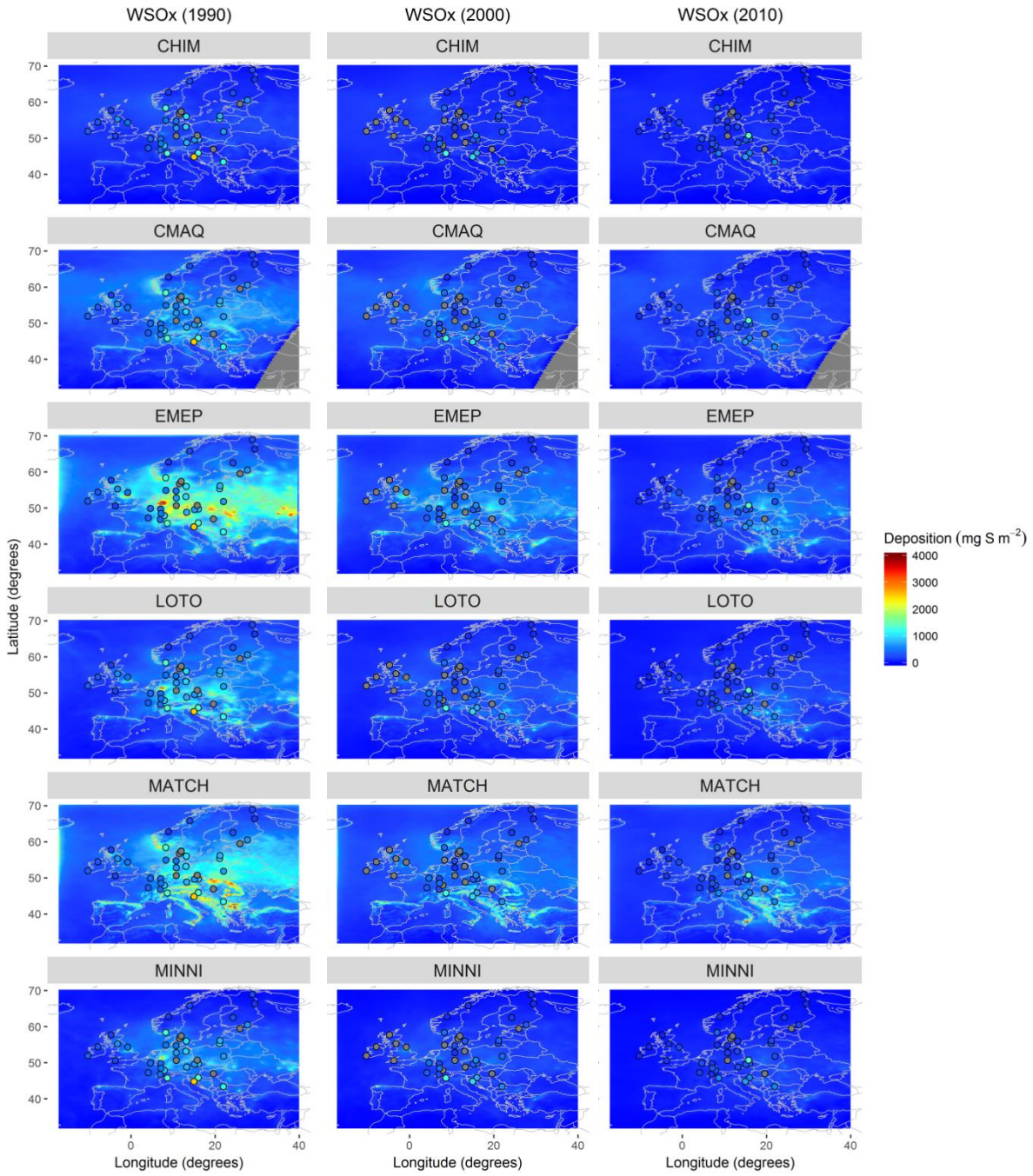

Figure S8: Accumulated annual WSOx deposition estimated by the six models for the years 1990 (left) and 2010 (right). The observed deposition is shown by the coloured circles (grey indicates no data).

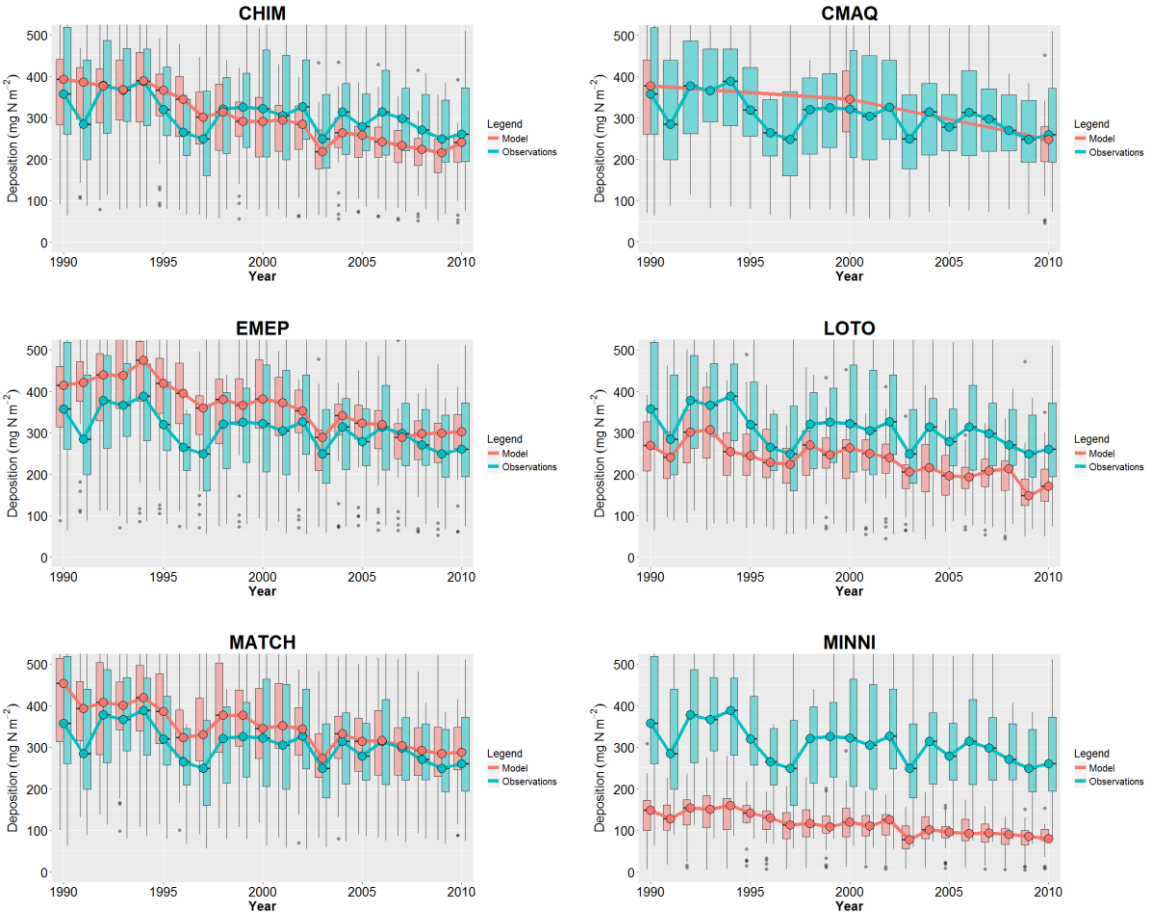

Figure S9: Tukey-style box plots of the time series of observed and modelled WNOx. Circles represent the annual median value for all measurement sites with a complete 21 year time series.

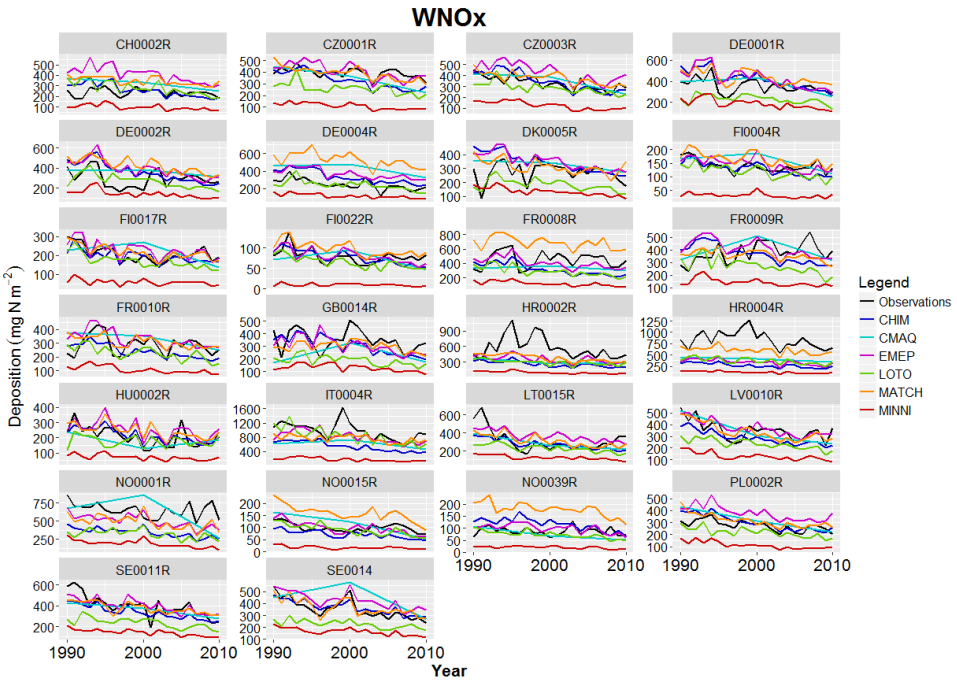

Figure S10: Time series of observed and modelled WNOx for all measurement sites with a complete 21 year time series.

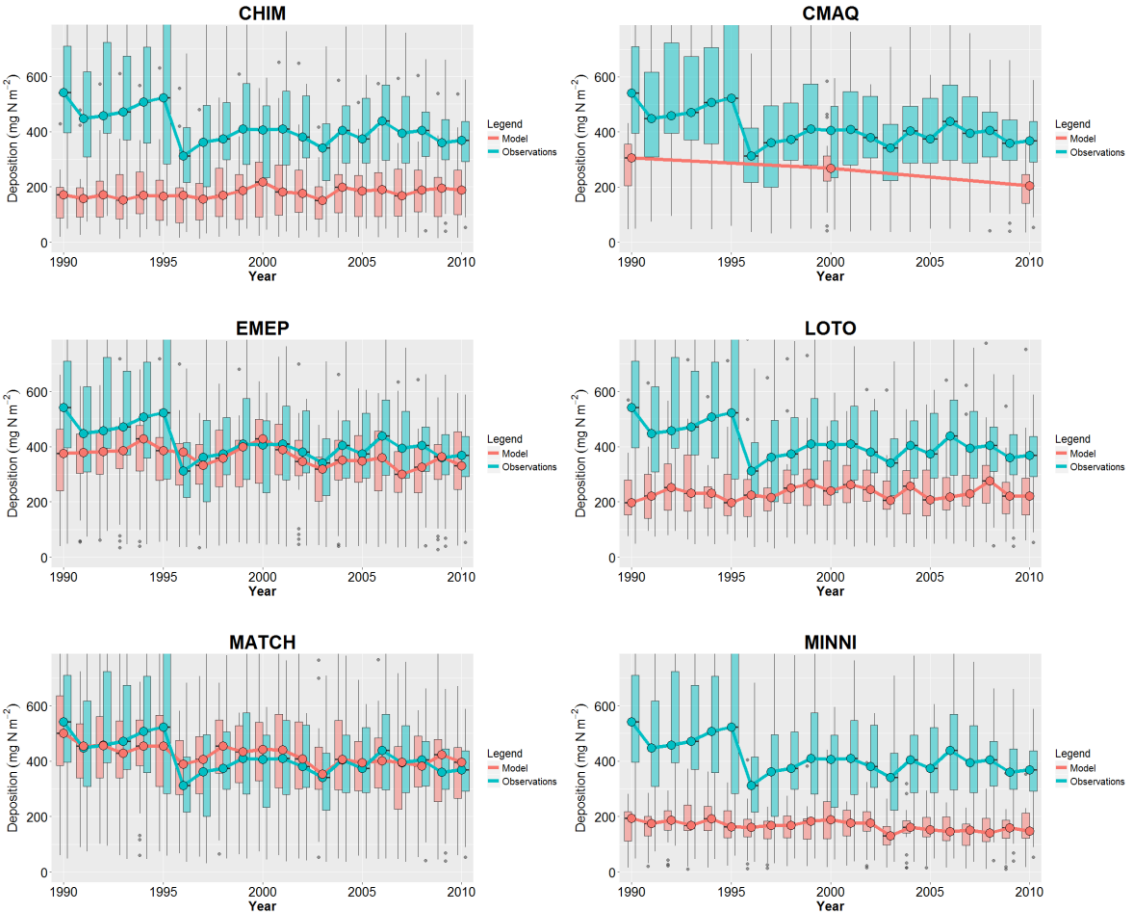

Figure S11: Tukey-style box plots of the time series of observed and modelled WNHx. Circles represent the annual median value for all measurement sites with a complete 21 year time series.

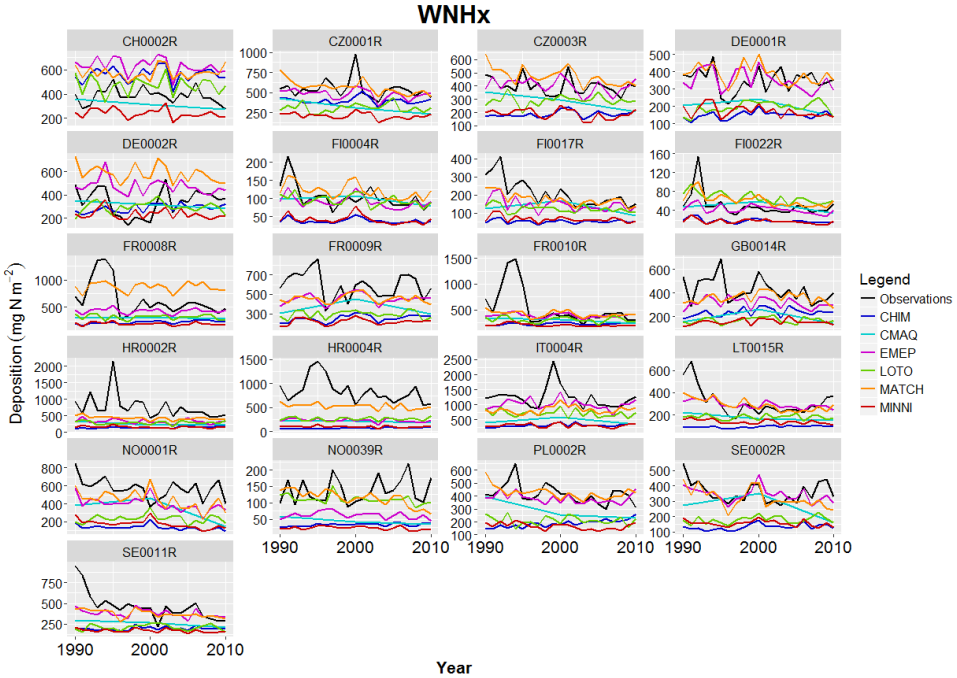

Figure S12: Time series of observed and modelled WNHx for all measurement sites with a complete 21 year time series.

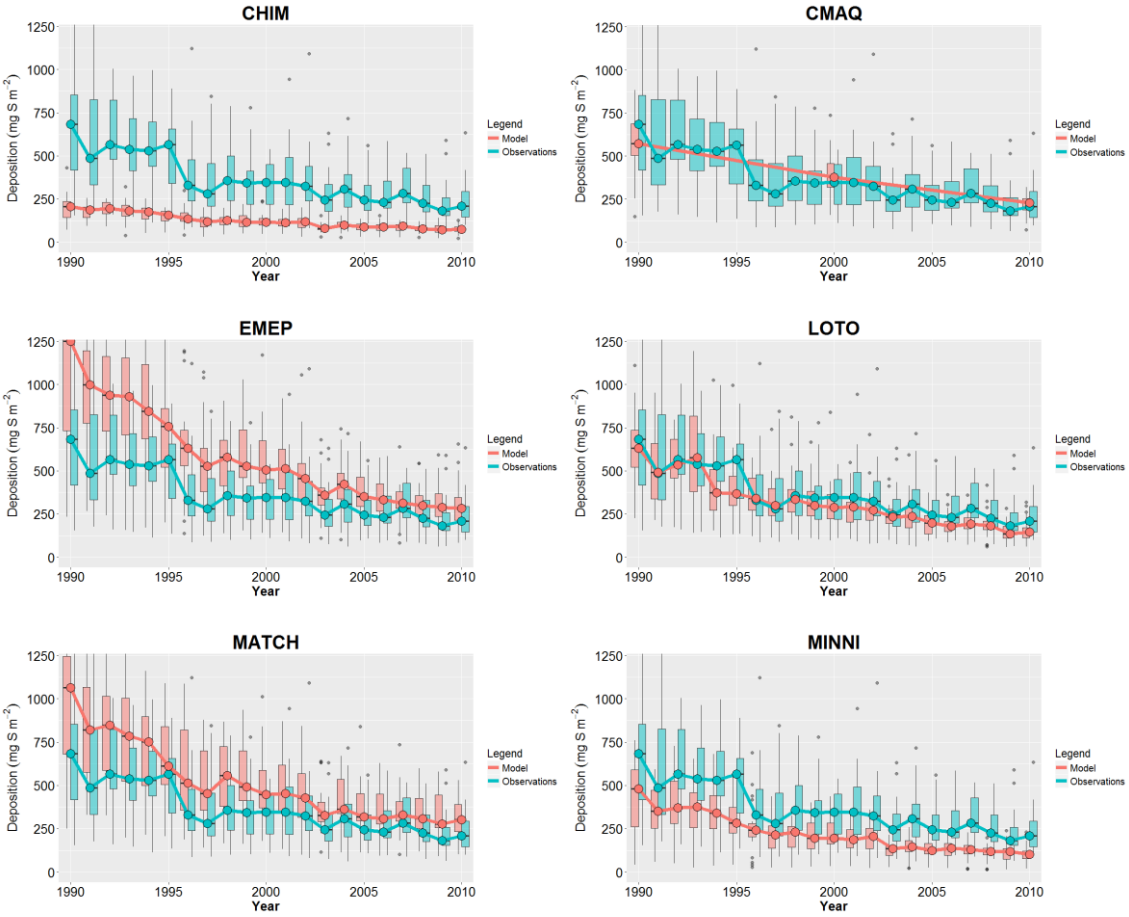

Figure S13: Tukey-style box plots of the time series of observed and modelled WSOx. Circles represent the annual median value for all measurement sites with a complete 21 year time series.

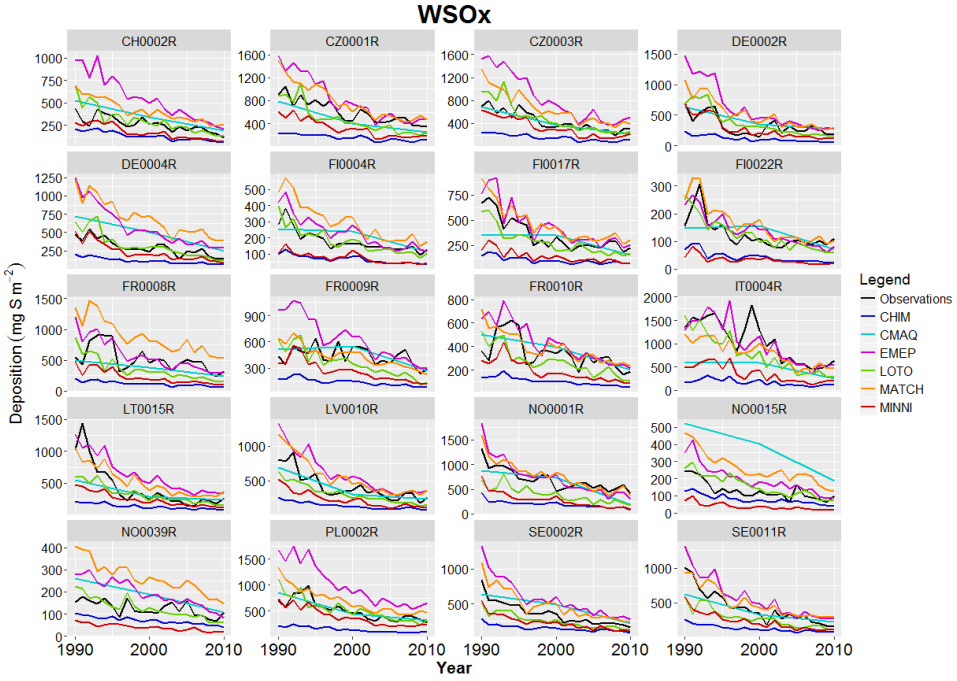

Figure S14: Time series of observed and modelled WSOx for all measurement sites with a complete 21 year time series.

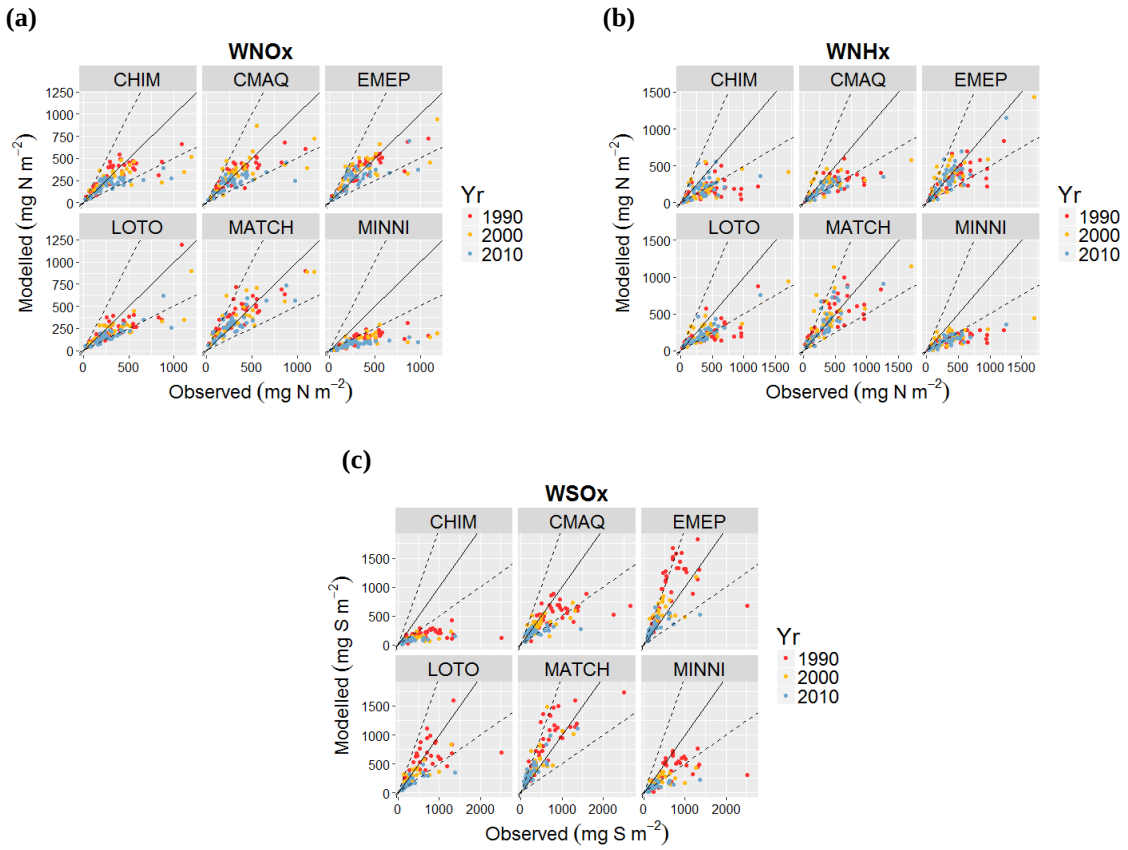

Figure S15: Modelled vs. observed wet deposition of a) WNOx, b) WNHx and c) WSOx for the years 1990, 2000 and 2010 (colour scale).

Table S3: Performance evaluation of the six models that simulated the individual years 1990, 2000 and 2010 and the five models that simulated the full 21 year time series for the three deposition components WNOx, WNHx and WSOx. Values meeting the acceptability criteria of Chang and Hanna (2004) are highlighted in bold green text. FAC2 is the fraction of model predictions within a factor of two of the observations, MG is the geometric mean bias, VG is the geometric variance, FB is the fractional bias, NMSE is the normalised mean squared error and r is the Pearson correlation coefficient.

		1990, 2000, 2010							21 year time series (1990-2010)						
Deposition Component	**Model**	n	FAC2	MG	VG	FB	NMSE	r	n	FAC2	MG	VG	FB	NMSE	r
WNOx	CHIM	108	**0.87**	**0.88**	**1.22**	**-0.23**	**0.41**	0.68	790	**0.89**	**0.87**	**1.24**	**-0.23**	**0.43**	0.63
	CMAQ	108	**0.93**	**0.96**	**1.18**	**-0.13**	**0.29**	0.72	-	-	-	-	-	-	-
	EMEP	108	**0.94**	**1.08**	**1.16**	**-0.02**	**0.21**	0.78	790	**0.90**	**1.07**	**1.17**	**-0.02**	**0.25**	0.71
	LOTO	108	**0.77**	**0.71**	**1.32**	-0.42	**0.48**	0.79	790	**0.82**	**0.72**	**1.29**	-0.39	**0.48**	0.76
	MATCH	108	**0.89**	**1.20**	**1.22**	**0.06**	**0.15**	0.84	790	**0.88**	**1.18**	**1.21**	**0.06**	**0.17**	0.81
	MINNI	108	0.16	0.30	5.18	-1.05	2.71	0.65	790	0.16	0.30	5.45	-1.06	2.81	0.59
WNHx	CHIM	103	0.41	0.45	**2.94**	-0.73	**1.49**	0.45	758	0.41	0.45	**3.02**	-0.74	1.64	0.35
	CMAQ	103	**0.68**	0.63	**1.56**	-0.54	**0.84**	0.68	-	-	-	-	-	-	-
	EMEP	103	**0.83**	**0.89**	**1.27**	**-0.15**	**0.25**	0.78	758	**0.82**	**0.88**	**1.30**	**-0.18**	**0.38**	0.66
	LOTO	103	**0.67**	0.66	**1.59**	-0.52	**0.71**	0.75	758	**0.68**	0.67	**1.54**	-0.52	**0.82**	0.67
	MATCH	103	**0.86**	**1.13**	**1.26**	**0.05**	**0.25**	0.72	758	**0.87**	**1.13**	**1.26**	**0.04**	**0.30**	0.66
	MINNI	103	0.34	0.40	**2.96**	-0.88	1.82	0.72	758	0.30	0.39	**3.22**	-0.92	2.10	0.63
WSOx	CHIM	97	0.23	0.32	4.82	-1.12	3.96	0.55	724	0.20	0.32	4.85	-1.13	3.78	0.55
	CMAQ	97	**0.76**	**0.73**	**1.38**	-0.42	**0.76**	0.66	-	-	-	-	-	-	-
	EMEP	97	**0.76**	1.34	**1.31**	**0.27**	**0.51**	0.65	724	**0.83**	1.31	**1.29**	**0.22**	**0.38**	0.67
	LOTO	97	**0.86**	**0.77**	**1.27**	**-0.26**	**0.54**	0.70	724	**0.85**	**0.76**	**1.28**	-0.32	**0.51**	0.74
	MATCH	97	**0.85**	1.41	**1.28**	**0.26**	**0.27**	0.83	724	**0.86**	1.35	**1.25**	**0.22**	**0.22**	0.83
	MINNI	97	**0.51**	0.47	**2.42**	-0.65	**1.33**	0.64	724	0.48	0.46	**2.47**	-0.70	**1.39**	0.64

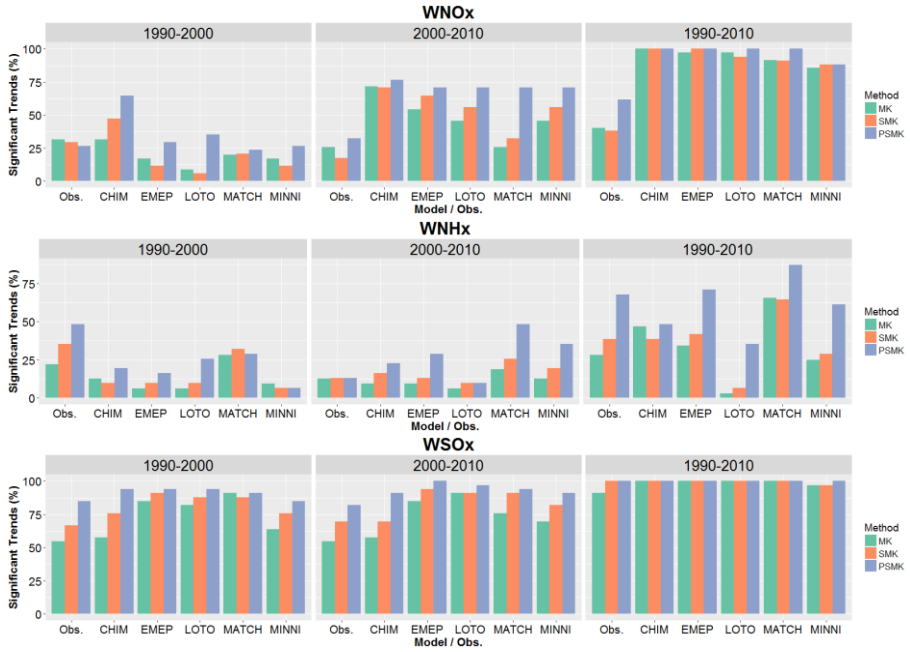

Figure S16: Proportion of observed/modelled trends that are significant for each trend estimation method (MK: Mann-Kendall; SMK: Seasonal Mann-Kendall; PSMK: Partial Seasonal Mann-Kendall) for WNOx (top), WNHx (middle) and WSOx (bottom) for the two 10 year periods and the full 20 year period.

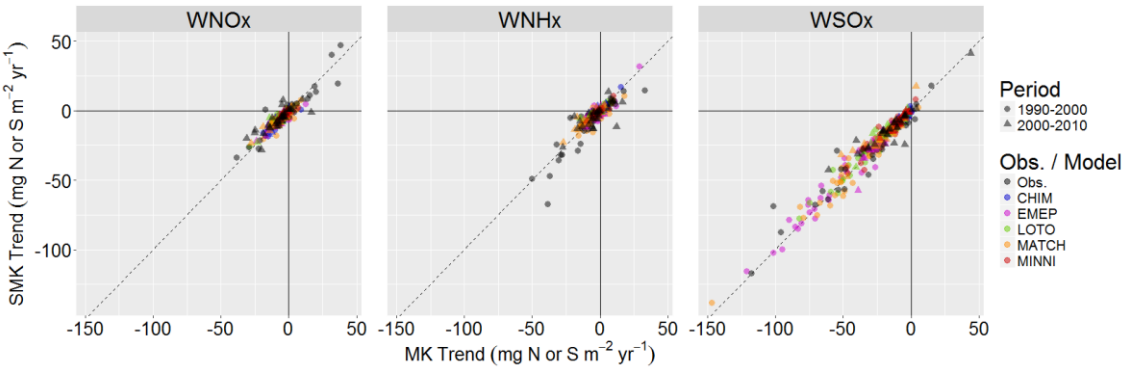

Figure S17: Observed/modelled absolute trends of WNOx, WNHx and WSOx calculated using the Seasonal Mann-Kendall (SMK) method versus those calculated using the Mann-Kendall (MK) method for the different time periods (symbols). The dashed line is the 1:1 line.

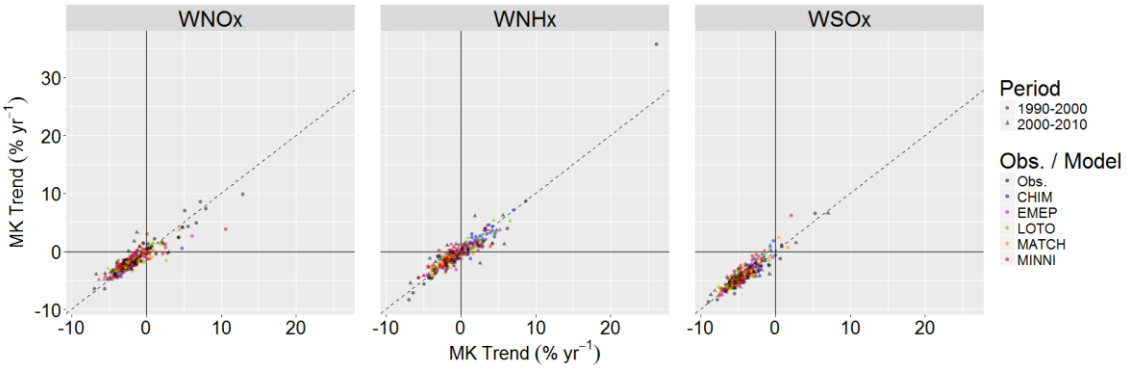

Figure S18: Observed/modelled relative trends of WNOx, WNHx and WSOx calculated using the Seasonal Mann-Kendall (SMK) method versus those calculated using the Mann-Kendall (MK) method for the different time periods (symbols). The dashed line is the 1:1 line.

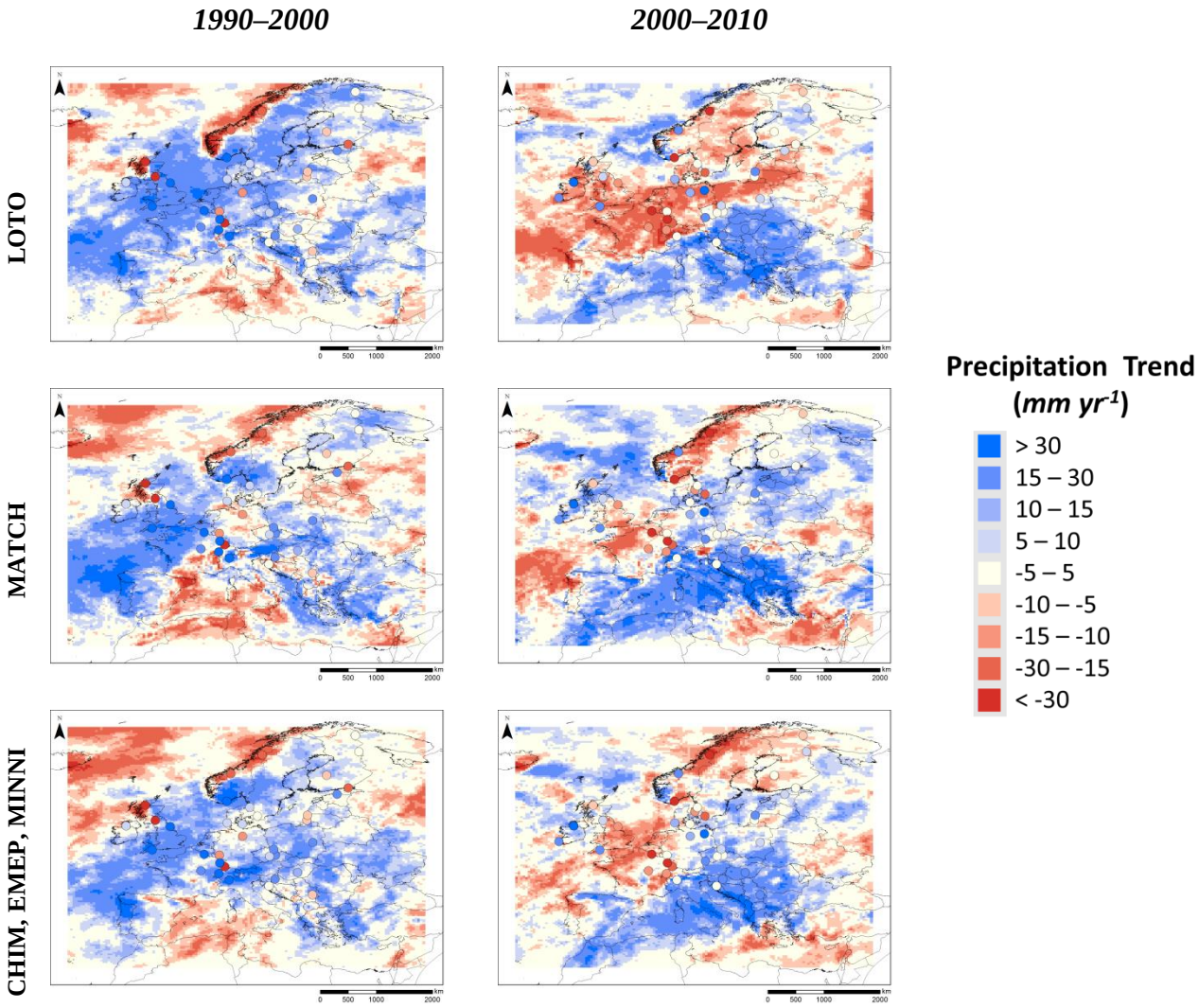

Figure S19: Maps of modelled (coloured field) and observed (circles) precipitation trends for the periods 1990-2000 and 2000–2010.

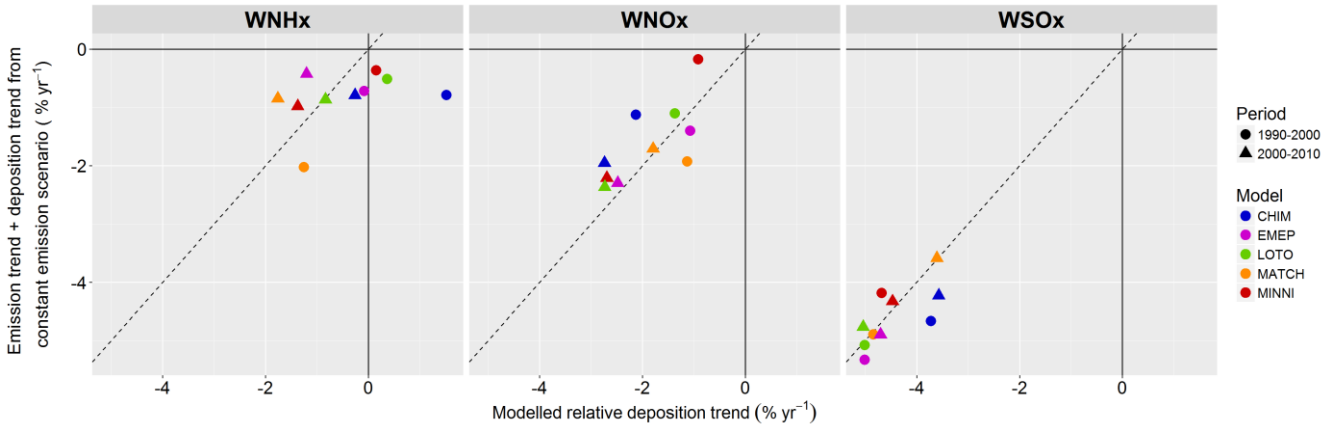

Figure S20: Scatter plots showing the sum of the median domain emission trends and the median wet deposition trends for the simulations with constant emissions vs. the median wet deposition trends for the simulations with changing emissions.

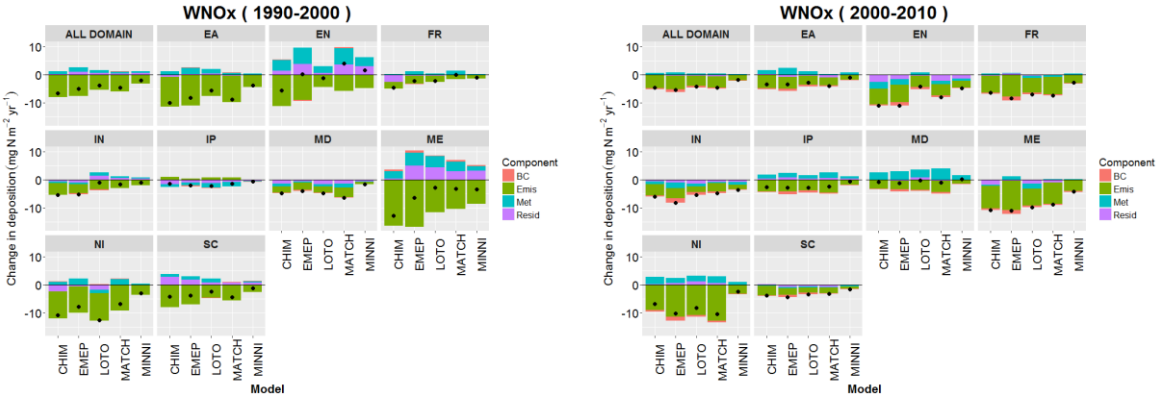

Figure S21: The mean contributions of the different factors (Bars) (BC: Boundary conditions; Emis: Emissions; Met: Meteorology and Resid: Residual interactions) to the WNOx trends (black circles) for all land grid cells for the entire domain and each subregion for the five models and two time periods.

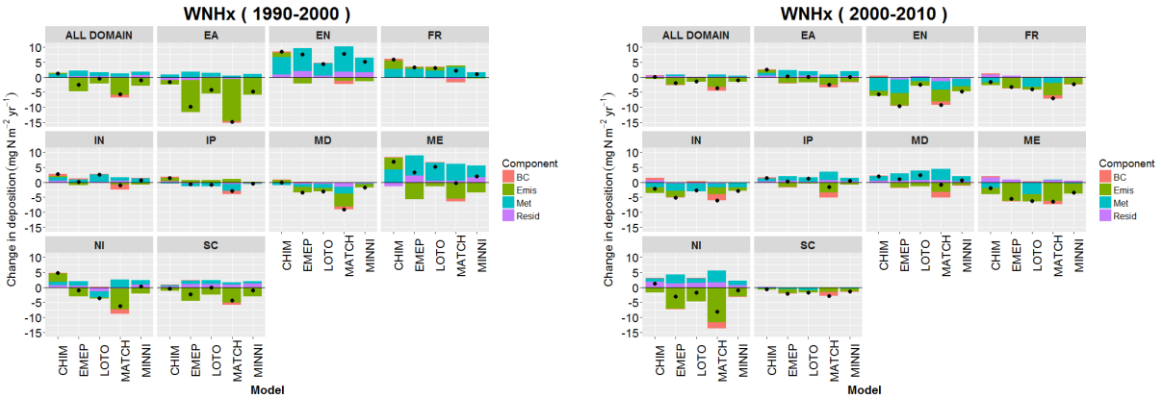

Figure S22: The mean contributions of the different factors (Bars) (BC: Boundary conditions; Emis: Emissions; Met: Meteorology and Resid: Residual interactions) to the WNHx trends (black circles) for all land grid cells for the entire domain and each subregion for the five models and two time periods.

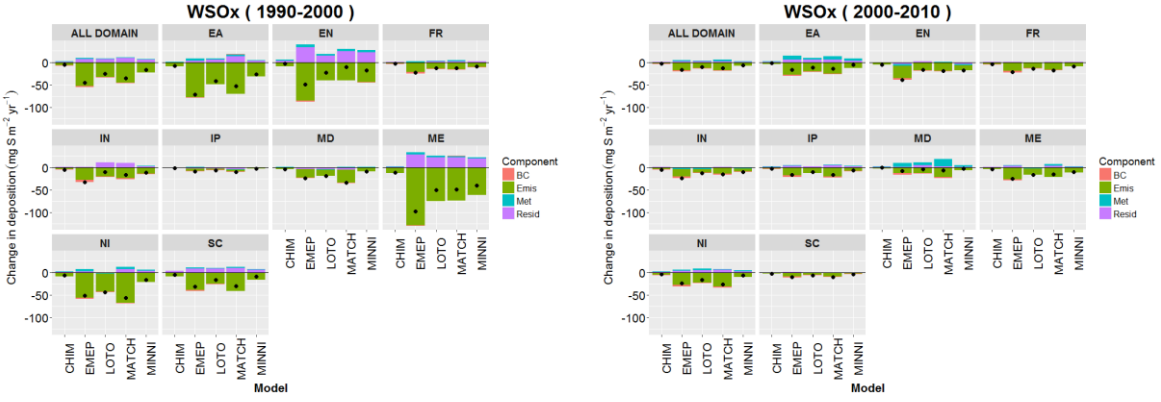

Figure S23: The mean contributions of the different factors (Bars) (BC: Boundary conditions; Emis: Emissions; Met: Meteorology and Resid: Residual interactions) to the WSOx trends (black circles) for all land grid cells for the entire domain and each subregion for the five models and two time periods.

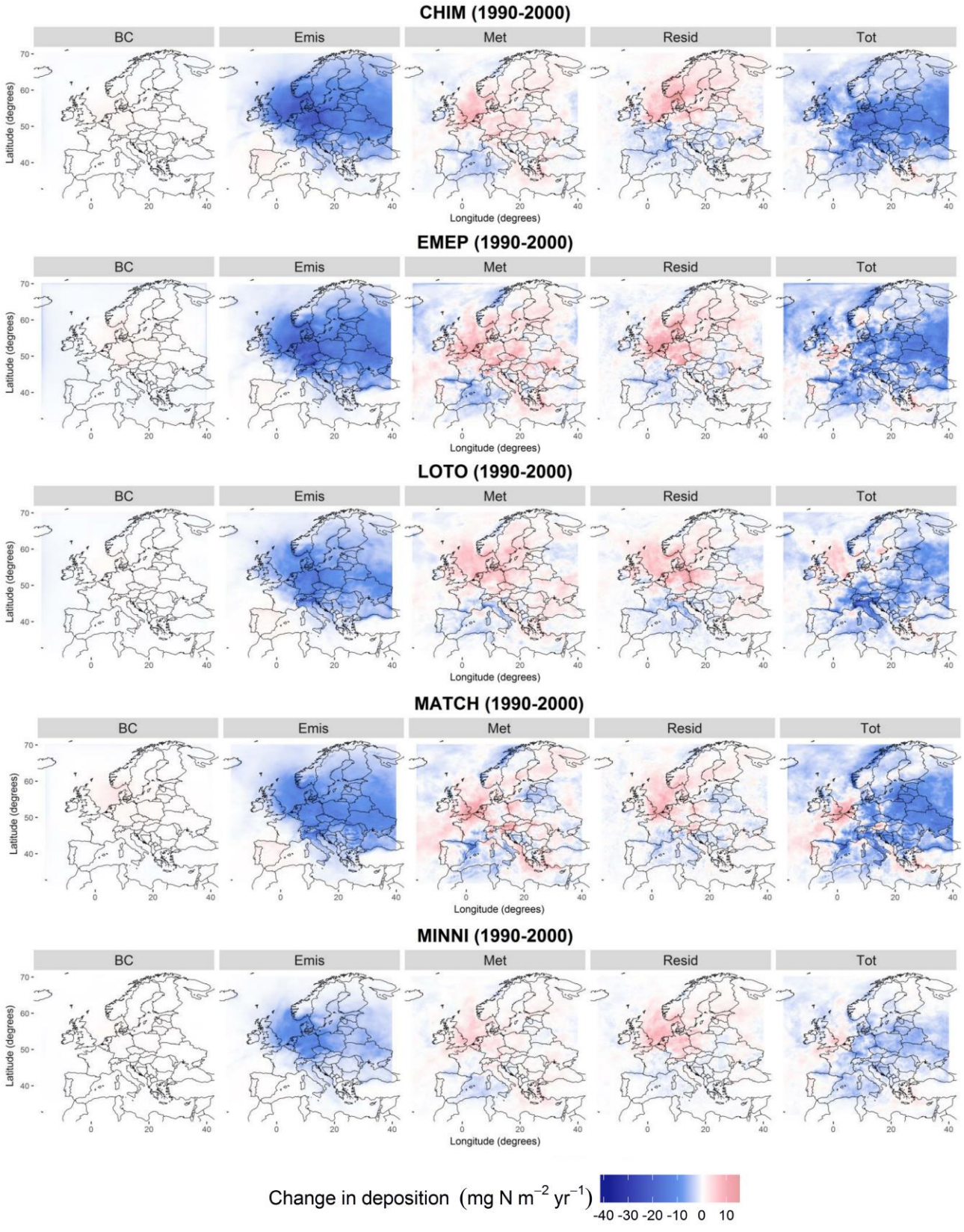

Figure S24: Spatial distributions of the contributions of the different factors (BC: Boundary conditions; Emis: Emissions; Met: Meteorology and Resid: Residual interactions) to the WNOx trends (Tot) for the period 1990-2000.

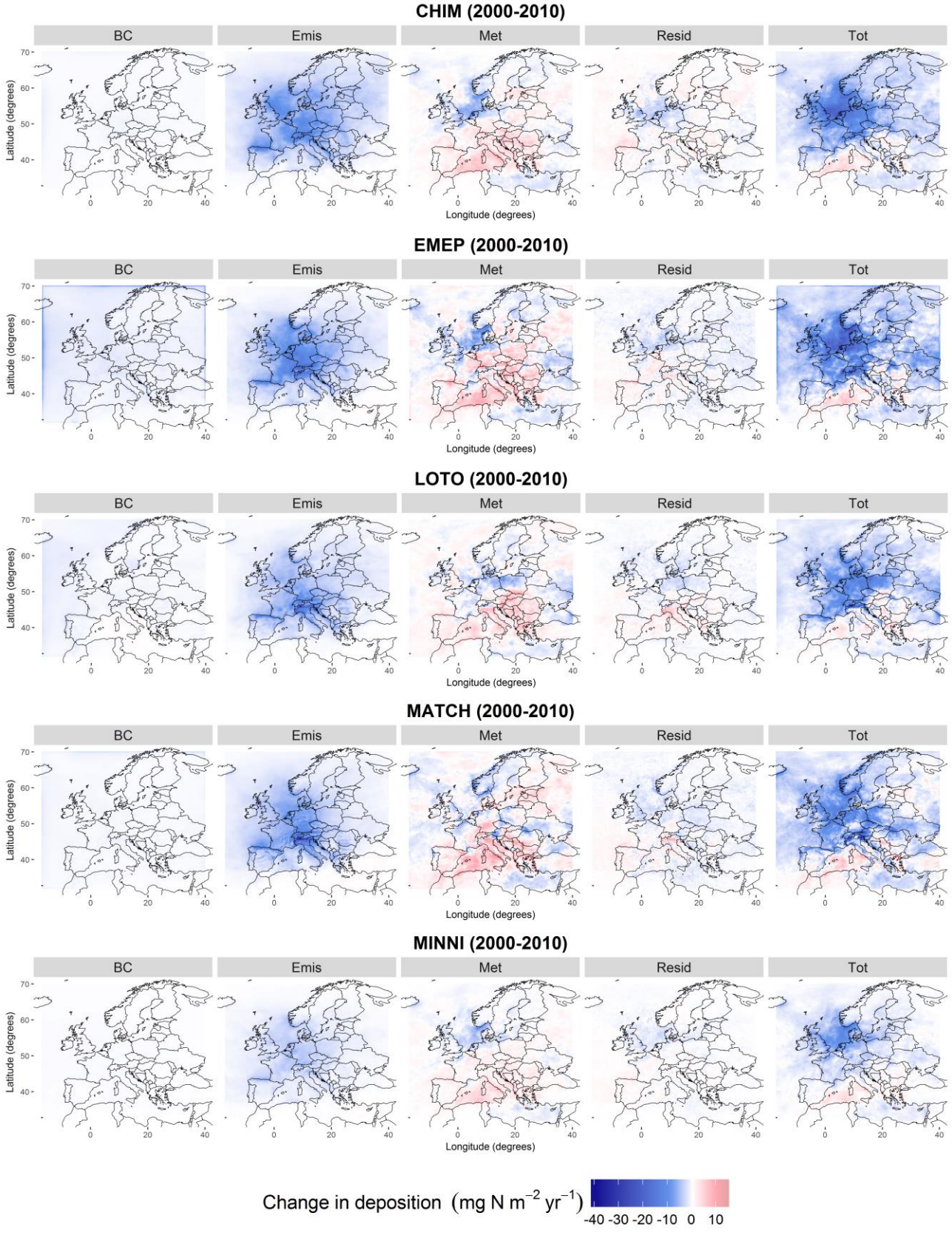

Figure S25: Spatial distributions of the contributions of the different factors (BC: Boundary conditions; Emis: Emissions; Met: Meteorology and Resid: Residual interactions) to the WNOx trends (Tot) for the period 2000-2010.

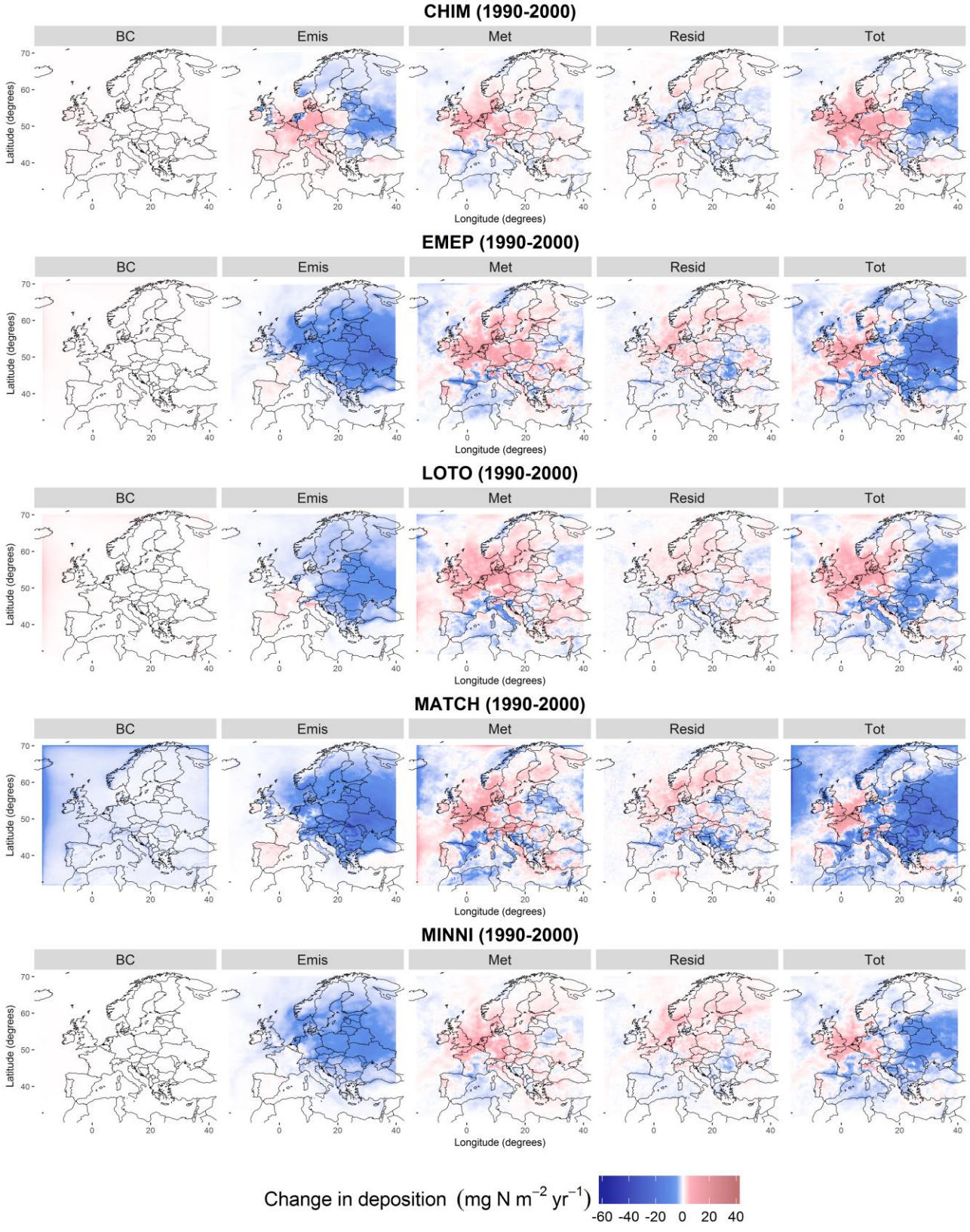

Figure S26: Spatial distributions of the contributions of the different factors (BC: Boundary conditions; Emis: Emissions; Met: Meteorology and Resid: Residual interactions) to the WNHx trends (Tot) for the period 1990-2000.

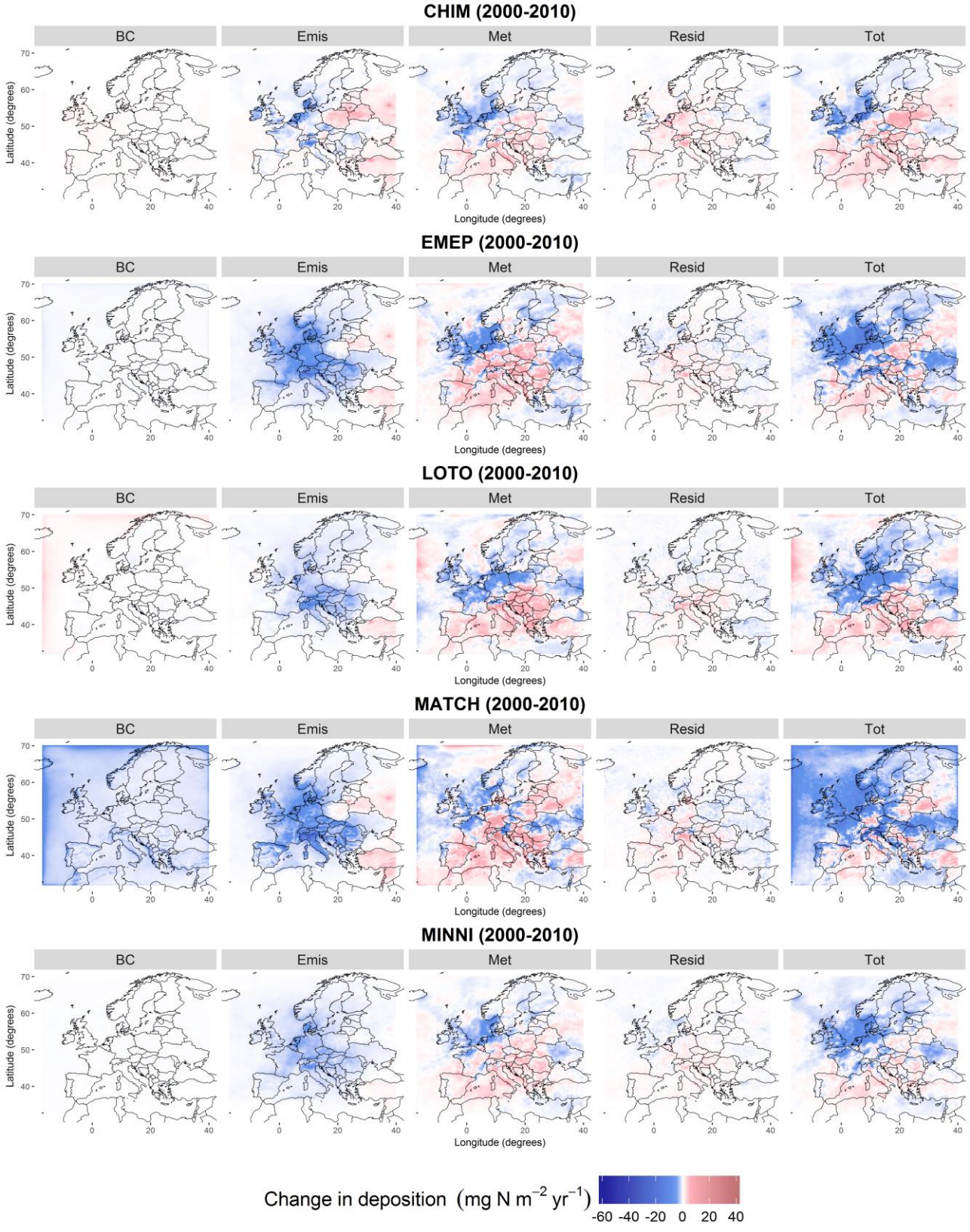

Figure S27: Spatial distributions of the contributions of the different factors (BC: Boundary conditions; Emis: Emissions; Met: Meteorology and Resid: Residual interactions) to the WNHx trends (Tot) for the period 2000-2010.

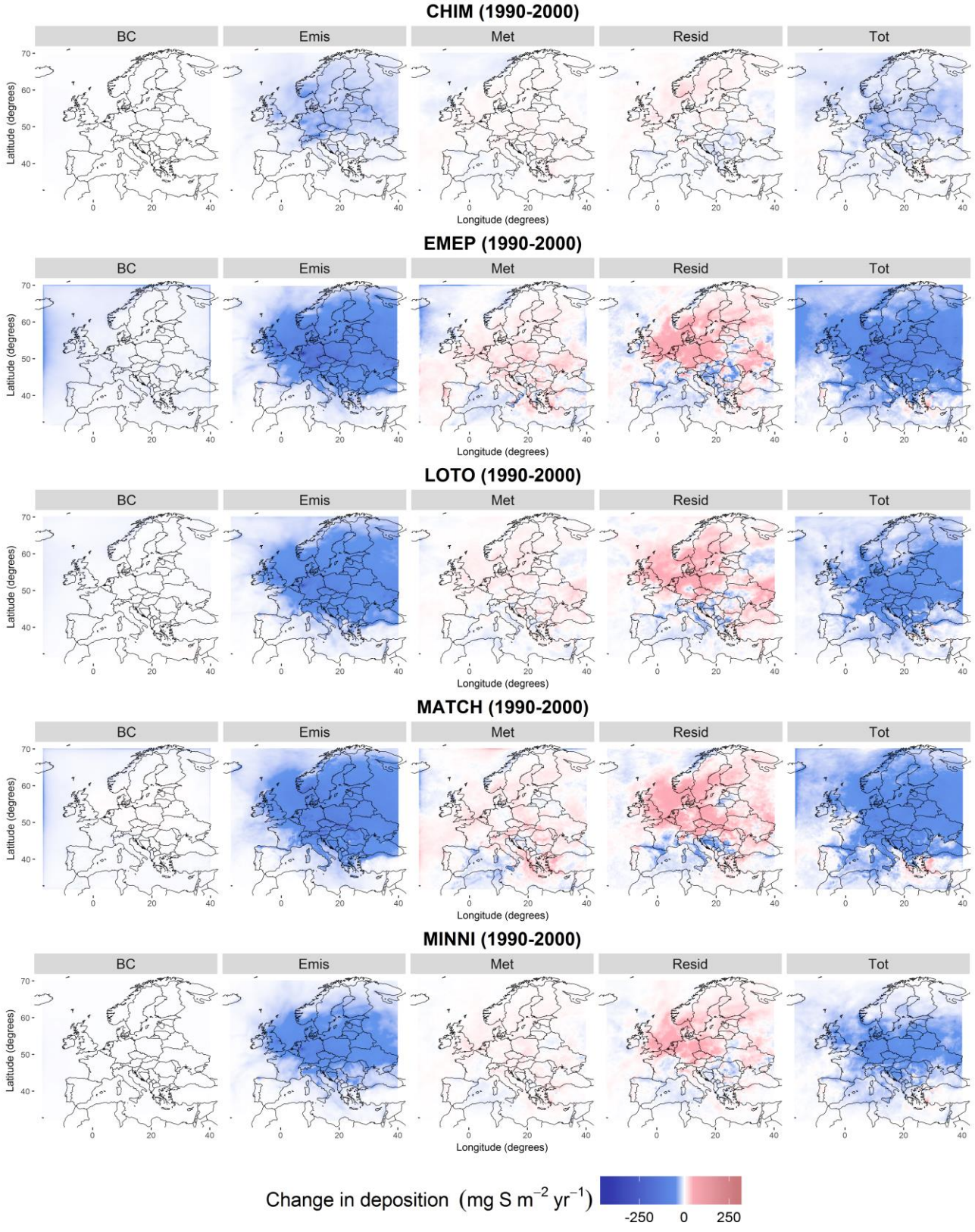

Figure S28: Spatial distributions of the contributions of the different factors (BC: Boundary conditions; Emis: Emissions; Met: Meteorology and Resid: Residual interactions) to the WSOx trends (Tot) for the period 1990-2000.

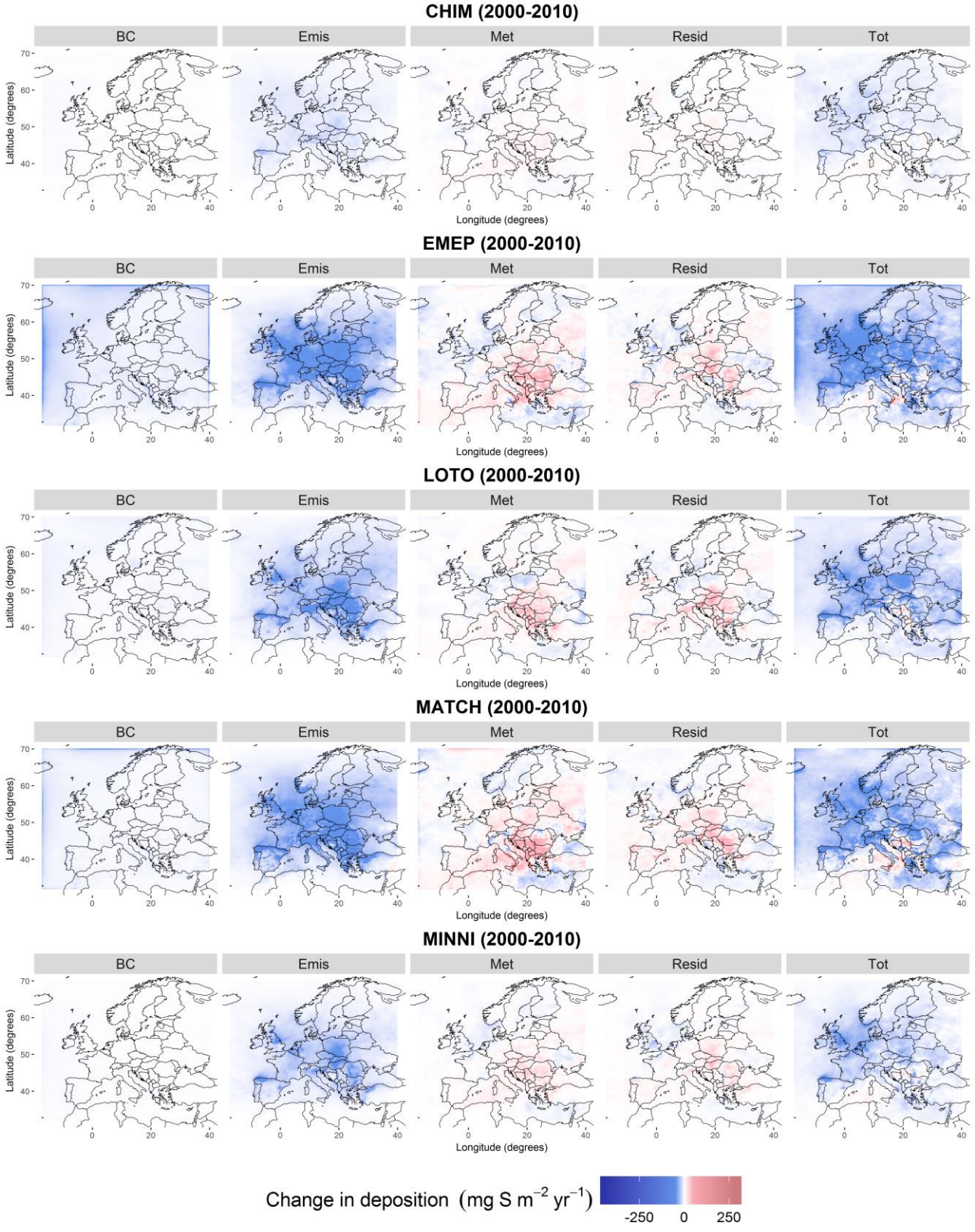

Figure S29: Spatial distributions of the contributions of the different factors (BC: Boundary conditions; Emis: Emissions; Met: Meteorology and Resid: Residual interactions) to the WSOx trends (Tot) for the period 2000-2010.

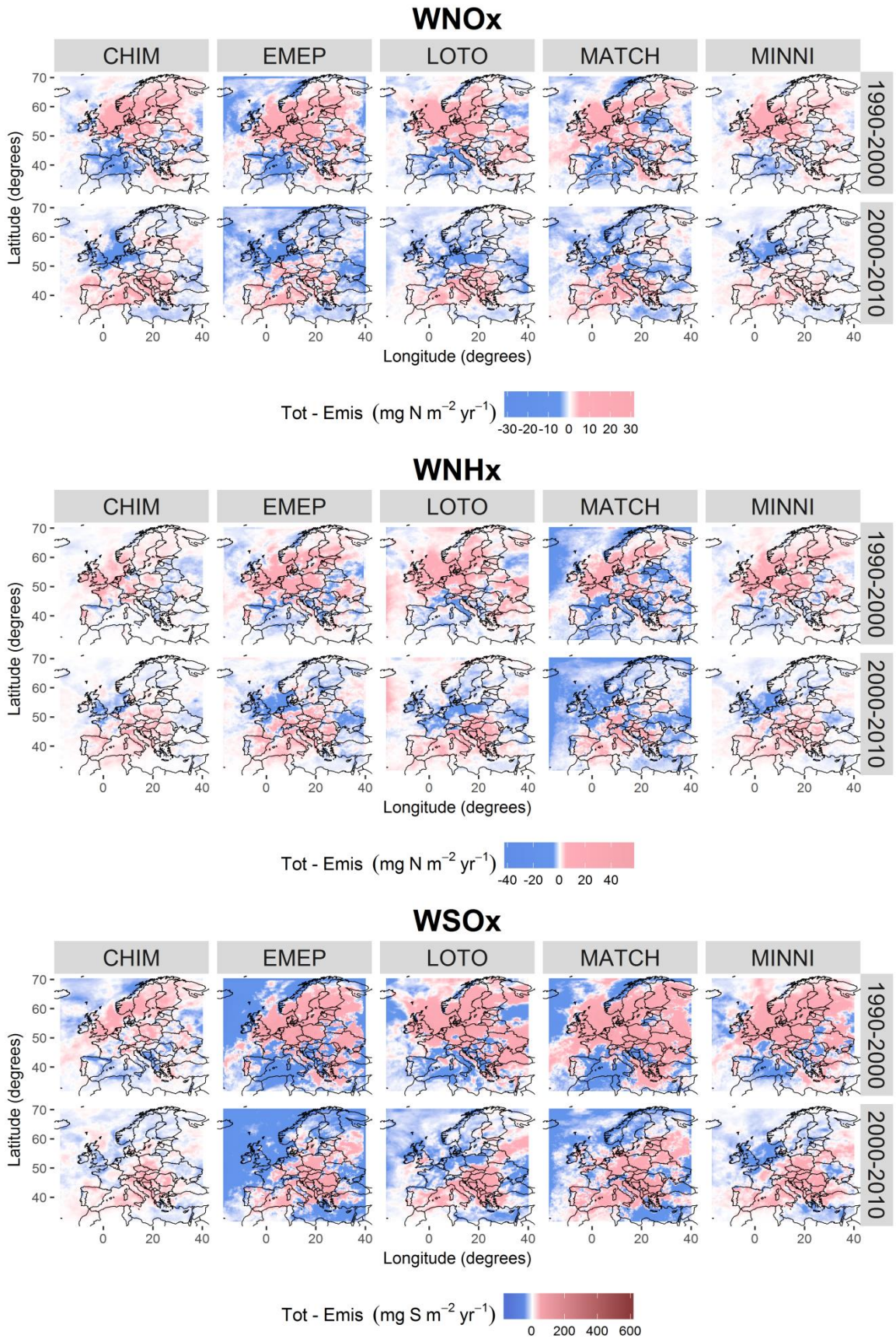

Figure S30: Spatial distributions of the sum of the factors not related to emissions (BC+Met+Resid, equal to Tot-Emis in the previous figures) for all deposition components, models and time periods. The offsetting of a decreasing trend due to emissions alone is shown as a positive value and the reinforcement of a decreasing trend is shown as a negative value.

Table S4: Performance evaluation of the seasonal and annual accumulated precipitation (at the wet deposition sites) used in the simulations of the six models that simulated the individual years 1990, 2000 and 2010 and the five models that simulated the full 21 year time series. Values meeting the acceptability criteria of Chang and Hanna (2004) are highlighted in bold green text. FAC2 is the fraction of model predictions within a factor of two of the observations, MG is the geometric mean bias, VG is the geometric variance, FB is the fractional bias, NMSE is the normalised mean squared error and r is the Pearson correlation coefficient.

		1990, 2000, 2010							21 year time series (1990-2010)						
Season	**Model**	n	FAC2	MG	VG	FB	NMSE	r	n	FAC2	MG	VG	FB	NMSE	r
Winter	CMAQ	108	**0.92**	**1.07**	**1.24**	**-0.02**	**0.21**	0.77	-	-	-	-	-	-	-
	LOTO	108	**0.92**	**1.06**	**1.23**	**0.00**	**0.21**	0.77	775	**0.75**	**1.04**	**1.45**	**-0.01**	**0.41**	0.53
	MATCH	108	**0.94**	**1.11**	**1.20**	**0.03**	**0.17**	0.81	775	**0.79**	**1.07**	**1.39**	**0.00**	**0.35**	0.58
	OTHERS	108	**0.90**	**1.09**	**1.29**	**0.01**	**0.24**	0.72	775	**0.75**	**1.09**	**1.45**	**0.00**	**0.43**	0.47
Spring	CMAQ	110	**0.89**	**0.93**	**1.26**	**-0.11**	**0.25**	0.67	-	-	-	-	-	-	-
	LOTO	110	**0.88**	**0.99**	**1.23**	**-0.03**	**0.17**	0.76	783	**0.82**	**1.04**	**1.36**	**-0.02**	**0.36**	0.50
	MATCH	110	**0.94**	**1.11**	**1.21**	**0.03**	**0.14**	0.77	783	**0.82**	**1.04**	**1.35**	**-0.03**	**0.35**	0.51
	OTHERS	110	**0.89**	**1.04**	**1.28**	**-0.03**	**0.26**	0.60	783	**0.79**	**1.01**	**1.41**	**-0.07**	**0.44**	0.36
Summer	CMAQ	110	**0.86**	**0.80**	**1.22**	**-0.21**	**0.19**	0.67	-	-	-	-	-	-	-
	LOTO	110	**0.75**	**0.72**	**1.50**	**-0.30**	**0.34**	0.46	776	**0.75**	**0.90**	**1.48**	**-0.10**	**0.34**	0.20
	MATCH	110	**0.92**	**1.02**	**1.16**	**0.01**	**0.16**	0.62	776	**0.78**	**1.01**	**1.39**	**0.00**	**0.29**	0.27
	OTHERS	110	**0.83**	**0.82**	**1.45**	**-0.16**	**0.26**	0.49	776	**0.72**	**0.80**	**1.67**	**-0.20**	**0.44**	0.08
Autumn	CMAQ	109	**0.89**	**0.89**	**1.19**	**-0.22**	**0.33**	0.80	-	-	-	-	-	-	-
	LOTO	109	**0.92**	**0.97**	**1.18**	**-0.12**	**0.22**	0.81	773	**0.82**	**0.94**	**1.41**	**-0.08**	**0.35**	0.51
	MATCH	109	**0.96**	**0.98**	**1.14**	**-0.10**	**0.18**	0.85	773	**0.84**	**0.93**	**1.31**	**-0.11**	**0.33**	0.56
	OTHERS	109	**0.84**	**0.91**	**1.23**	**-0.19**	**0.33**	0.75	773	**0.79**	**0.89**	**1.39**	**-0.16**	**0.44**	0.42
Annual	CMAQ	437	**0.89**	**0.92**	**1.23**	**-0.15**	**0.25**	0.74	-	-	-	-	-	-	-
	LOTO	437	**0.87**	**0.92**	**1.28**	**-0.11**	**0.24**	0.74	3868	**0.81**	**0.98**	**1.36**	**-0.06**	**0.32**	0.84
	MATCH	437	**0.94**	**1.05**	**1.17**	**-0.01**	**0.17**	0.79	3868	**0.84**	**1.01**	**1.31**	**-0.04**	**0.29**	0.85
	OTHERS	437	**0.86**	**0.96**	**1.31**	**-0.10**	**0.28**	0.67	3868	**0.79**	**0.94**	**1.42**	**-0.11**	**0.45**	0.78

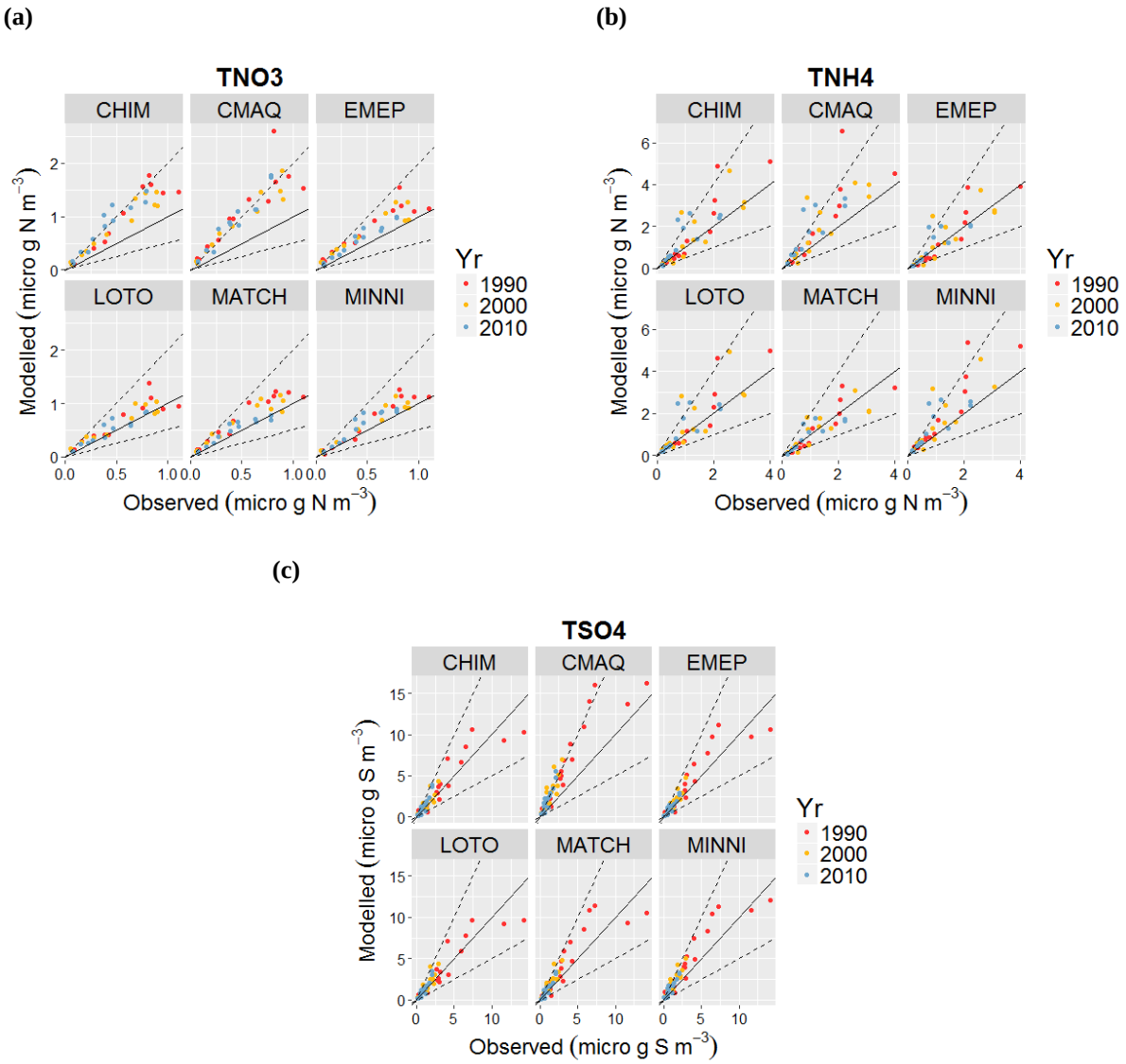

Figure S31: Modelled vs. observed mean annual concentrations of a) TNO3, b) TNH4 and c) TSO4 for the years 1990, 2000 and 2010 (colour scale).

Table S5: Performance evaluation of the six models that simulated the individual years 1990, 2000 and 2010 for the three atmospheric components TNO3, TNH4 and TSO4 at all sites and only at sites with wet deposition observations. Values meeting the acceptability criteria of Chang and Hanna (2004) are highlighted in bold green text. FAC2 is the fraction of model predictions within a factor of two of the observations, MG is the geometric mean bias, VG is the geometric variance, FB is the fractional bias, NMSE is the normalised mean squared error and r is the Pearson correlation coefficient.

		Atmospheric concentrations 1990, 2000, 2010								Wet deposition at concentration sites 1990, 2000, 2010						
Concentration Component	**Model**	n	FAC2	MG	VG	FB	NMSE	r	**Deposition Component**	n	FAC2	MG	VG	FB	NMSE	r
TNO3	CHIM	37	**0.73**	1.81	**1.48**	0.56	**0.49**	0.94	WNOx	30	**0.97**	**0.98**	**1.10**	**-0.07**	**0.09**	0.89
	CMAQ	37	0.30	2.15	**1.87**	0.69	**0.80**	0.92		30	**0.97**	**0.94**	**1.11**	**-0.08**	**0.12**	0.84
	EMEP	37	**0.89**	1.53	**1.28**	0.34	**0.18**	0.94		30	**1.00**	**1.10**	**1.09**	**0.06**	**0.08**	0.87
	LOTO	37	**0.95**	**1.29**	**1.15**	**0.17**	**0.09**	0.92		30	**0.80**	**0.71**	**1.25**	-0.43	**0.41**	0.87
	MATCH	37	**0.95**	1.37	**1.16**	**0.26**	**0.13**	0.94		30	**0.93**	**1.16**	**1.16**	**0.05**	**0.09**	0.87
	MINNI	37	**0.97**	**1.25**	**1.10**	**0.22**	**0.10**	0.96		30	0.10	0.31	5.11	-0.95	1.58	0.89
TNH4	CHIM	39	**0.85**	**1.17**	**1.21**	**0.27**	**0.37**	0.87	WNHx	32	0.22	0.36	**3.43**	-0.93	1.74	0.69
	CMAQ	39	**0.82**	1.47	**1.35**	0.44	**0.57**	0.83		32	**0.59**	0.55	**1.70**	-0.61	**0.80**	0.69
	EMEP	39	**0.92**	**0.96**	**1.20**	**0.09**	**0.20**	0.87		32	**0.88**	**0.77**	**1.25**	**-0.24**	**0.27**	0.75
	LOTO	39	**0.90**	**1.19**	**1.20**	**0.24**	**0.37**	0.84		32	**0.63**	0.58	**1.72**	-0.65	**1.02**	0.54
	MATCH	39	**0.87**	**0.86**	**1.23**	**-0.03**	**0.17**	0.87		32	**0.91**	**0.97**	**1.16**	**-0.02**	**0.29**	0.66
	MINNI	39	**0.90**	1.39	**1.27**	0.37	**0.44**	0.86		32	0.25	0.35	**3.54**	-0.91	1.64	0.72
TSO4	CHIM	54	**0.85**	**1.24**	**1.24**	**0.14**	**0.24**	0.92	WSOx	56	0.25	0.36	**3.46**	-1.05	2.94	0.77
	CMAQ	54	0.46	2.00	**1.87**	0.59	**0.78**	0.92		56	**0.84**	**0.99**	**1.29**	**-0.16**	**0.40**	0.70
	EMEP	54	**0.89**	**1.19**	**1.20**	**0.17**	**0.25**	0.92		56	**0.80**	1.42	**1.29**	0.36	**0.39**	0.82
	LOTO	54	**0.89**	**1.20**	**1.20**	**0.10**	**0.24**	0.92		56	**0.91**	**0.83**	**1.20**	**-0.18**	**0.32**	0.79
	MATCH	54	**0.87**	**1.26**	**1.27**	**0.24**	**0.36**	0.89		56	**0.86**	1.47	**1.26**	**0.30**	**0.24**	0.87
	MINNI	54	**0.80**	1.55	**1.43**	0.33	**0.30**	0.93		56	**0.55**	0.50	**2.09**	-0.56	**0.80**	0.79

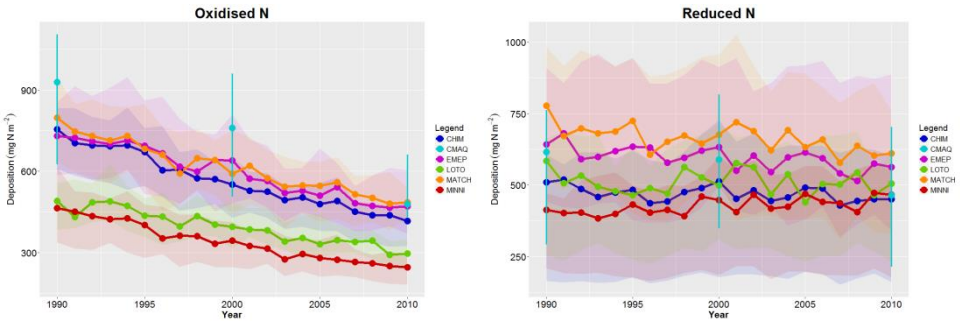

Figure S32: Time series of modelled total deposition (wet plus dry) of oxidised N (left) and reduced N (right) at the measurement sites. Points represent the median value for all measurement sites and the shading (or error bars) represents the interquartile range.

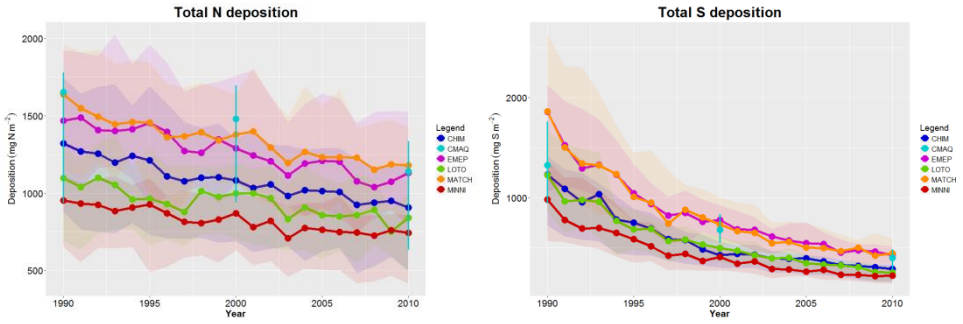

Figure S33: Time series of modelled total deposition (wet plus dry) of nitrogen (left) and sulphur (right) at the measurement sites. Points represent the median value for all measurement sites and the shading (or error bars) represents the interquartile range.

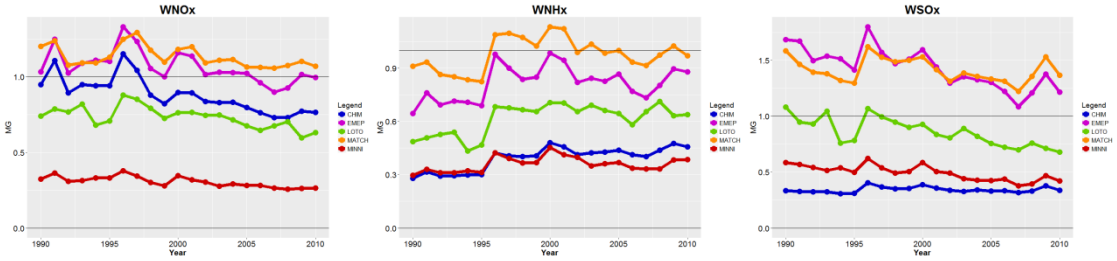

Figure S34: Time series of model geometric mean bias for WNOx, WNHx and WSOx.

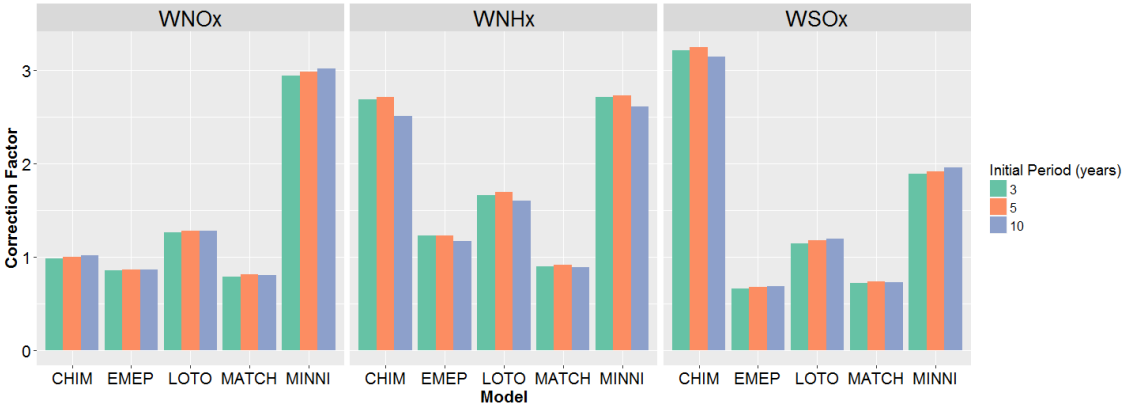

Figure S35: Bias correction factors for different lengths of initial period used for the bias correction.

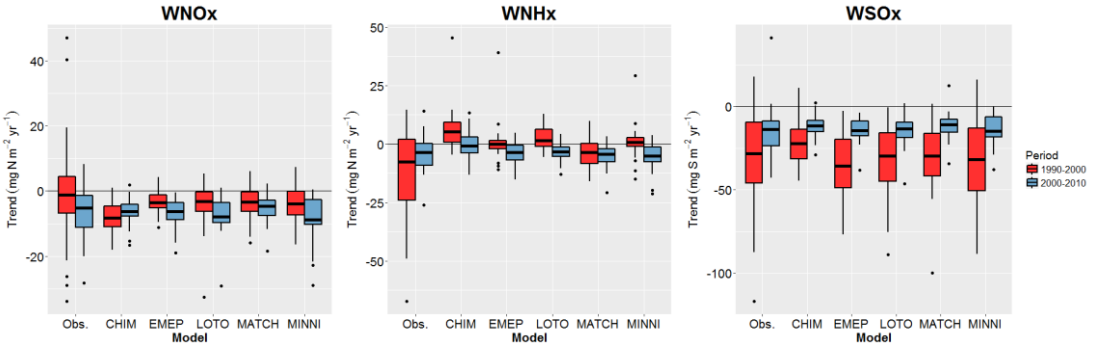

Figure S36: Tukey-style box plots of observed and bias-corrected (3 year initial period) modelled absolute trends for WNOx, WNHx, WSOx for the two periods 1990-2000 and 2000-2010.

References cited in the Supplementary Material

Andersson, C., Langner, J. and Bergström, R.: Interannual variation and trends in air pollution over Europe due to climate variability during 1958–2001 simulated with a regional CTM coupled to the ERA40 reanalysis, Tellus B, 59, 77-98, 2007.

Banzhaf, S., Schaap, M., Kerschbaumer, A., Reimer, E., Stern, R., Van Der Swaluw, E. and Builtjes, P.: Implementation and evaluation of pH-dependent cloud chemistry and wet deposition in the chemical transport model REM-Calgrid, Atmos. Environ., 49, 378-390, 2012.

Berge, E.: Coupling of wet scavenging of sulphur to clouds in a numerical weather prediction model, Tellus B, 45, 1-22, 1993.

Binkowski, F. S. and Shankar, U.: The regional particulate matter model: 1. Model description and preliminary results, Journal of Geophysical Research: Atmospheres, 100, 26191-26209, 1995.

Byun, D. and Schere, K. L.: Review of the governing equations, computational algorithms, and other components of the Models-3 Community Multiscale Air Quality (CMAQ) modeling system, Appl. Mech. Rev., 59, 51-77, 2006.

Carter, W. P.: Documentation of the SAPRC-99 chemical mechanism for VOC reactivity assessment, Contract, 92, 95-308, 2000.

Carter, W. P.: Condensed atmospheric photooxidation mechanisms for isoprene, Atmos. Environ., 30, 4275-4290, 1996.

Chang, J., Brost, R., Isaksen, I., Madronich, S., Middleton, P., Stockwell, W. and Walcek, C.: A three- dimensional Eulerian acid deposition model: Physical concepts and formulation, Journal of Geophysical Research: Atmospheres, 92, 14681-14700, 1987.

Emberson, L., Simpson, D., Tuovinen, J., Ashmore, M. and Cambridge, H.: Towards a model of ozone deposition and stomatal uptake over Europe, EMEP MSC-W Note, 6, 1-57, 2000a.

Emberson, L., Ashmore, M., Cambridge, H., Simpson, D. and Tuovinen, J.: Modelling stomatal ozone flux across Europe, Environmental Pollution, 109, 403-413, 2000b.

Langner, J., Bergström, R. and Pleijel, K. 1998. European scale modelling of sulphur, oxidized nitrogen and photochemical oxidants. Model development and evaluation for the 1994 growing season, SMHI report, RMKNo. 82, Swedish Met. and Hydrol. Inst., Norrk¨oping, Sweden

Menut, L., Bessagnet, B., Khvorostyanov, D., Beekmann, M., Blond, N., Colette, A., Coll, I., Curci, G., Foret, G. and Hodzic, A.: CHIMERE 2013: a model for regional atmospheric composition modelling, Geoscientific model development, 6, 981-1028, 2013.

Mozurkewich, M.: The dissociation constant of ammonium nitrate and its dependence on temperature, relative humidity and particle size, Atmospheric Environment.Part A.General Topics, 27, 261-270, 1993.

Nenes, A., Pandis, S. N. and Pilinis, C.: Continued development and testing of a new thermodynamic aerosol module for urban and regional air quality models, Atmos. Environ., 33, 1553-1560, 1999.

Pleim, J. E. and Xiu, A.: Development and testing of a surface flux and planetary boundary layer model for application in mesoscale models, J. Appl. Meteor., 34, 16–32, 1995.

Pleim, J. E. and Xiu, A.: Development of a land surface model. Part II: Data assimilation. J. Appl. Meteorol.Climatol. 2003, 42, 1811–1822.

Pleim, J.E., Bash, J.O., Walker, J.T., & Cooter, E.J. (2013). Development and testing of an ammonia bi-directional flux model for air-quality models, J. Geophys. Res. 118, doi: 10.1002/jgrd.50262.

Scott, B.: Parameterization of sulfate removal by precipitation, J. Appl. Meteorol., 17, 1375-1389, 1978.

Seinfeld, J. H. and Pandis, S. N.: From air pollution to climate change, Atmospheric Chemistry and Physics, John Wiley & Sons, New York, 1326, 1998.

Simpson, D., Fagerli, H., Jonson, J., Tsyro, S. and Wind, P.:, Transboundary Acidification, Eutrophication and Ground Level Ozone in Europe.Part I-Unified EMEP Model Description. Norwegian Meteorological Institute, Oslo, 2003.

Simpson, D., Benedictow, A., Berge, H., Bergström, R., Emberson, L. D., Fagerli, H., Flechard, C. R., Hayman, G. D., Gauss, M. and Jonson, J. E.: The EMEP MSC-W chemical transport model–technical description, Atmospheric Chemistry and Physics, 12, 7825-7865, 2012.

Strand, A. and Hov, Ø.: A two-dimensional global study of tropospheric ozone production, Journal of Geophysical Research: Atmospheres, 99, 22877-22895, 1994.

Tuovinen, J., Ashmore, M., Emberson, L. and Simpson, D.: Testing and improving the EMEP ozone deposition module, Atmos. Environ., 38, 2373-2385, 2004.

Van Zanten, M., Sauter, F., RJ, W. K., Van Jaarsveld, J. and Van Pul, W.: Description of the DEPAC module: Dry deposition modelling with DEPAC_GCN2010, RIVM rapport 680180001, 2010.

Venkatram, A. and Pleim, J.: The electrical analogy does not apply to modeling dry deposition of particles, Atmos. Environ., 33, 3075-3076, 1999.

Walcek, C. J. and Taylor, G. R.: A theoretical method for computing vertical distributions of acidity and sulfate production within cumulus clouds, J. Atmos. Sci., 43, 339-355, 1986.

Wesely, M.: Parameterization of surface resistances to gaseous dry deposition in regional-scale numerical models, Atmospheric Environment (1967), 23, 1293-1304, 1989.

Wichink Kruit, R., Schaap, M., Sauter, F., Van der Swaluw, E. and Weijers, E.: Improving the understanding of the secondary inorganic aerosol distribution over the Netherlands, TNO Rep.TNO-060-UT-2012, 334, 2012.
Yarwood, G., Rao, S., Yocke, M. and Whitten, G.: Updates to the carbon bond chemical mechanism: CB05, Final report to the US EPA, RT-0400675, 8, 2005.
Zhang, L., Gong, S., Padro, J. and Barrie, L.: A size-segregated particle dry deposition scheme for an atmospheric aerosol module, Atmos. Environ., 35, 549-560, 2001.